CENTRAL RESEARCH LIBRARY
DOCUMENT COLLECTION

MARTIN MARIETTA ENERGY SYSTEMS LIBRARIES
3 4456 0349518 0

ORNL 1537
Physics

Cy. 4A

DETERMINATION OF THE POWER OF THE BULK SHIELDING REACTOR – PART III MEASUREMENT OF THE ENERGY RELEASED PER FISSION

J. L. Meem
L. B. Holland
G. M. McCammon

CENTRAL RESEARCH LIBRARY
DOCUMENT COLLECTION

LIBRARY LOAN COPY

DO NOT TRANSFER TO ANOTHER PERSON

If you wish someone else to see this document, send in name with document and the library will arrange a loan.

OAK RIDGE NATIONAL LABORATORY
OPERATED BY
CARBIDE AND CARBON CHEMICALS COMPANY
A DIVISION OF UNION CARBIDE AND CARBON CORPORATION

UCC

POST OFFICE BOX P
OAK RIDGE, TENNESSEE

ORNL 1537

This document consists of 88 pages.
Copy 4 of 330 copies. Series A.

Contract No. W-7405-eng-26

PHYSICS DIVISION

DETERMINATION OF THE POWER OF THE BULK SHIELDING REACTOR -- PART III

MEASUREMENT OF THE ENERGY RELEASED PER FISSION

J. L. Meem L. B. Holland
G. M. McCammon

DATE ISSUED

FEB 15 1954

OAK RIDGE NATIONAL LABORATORY
Operated by
CARBIDE AND CARBON CHEMICALS COMPANY
A Division of Union Carbide and Carbon Corporation
Post Office Box P
Oak Ridge, Tennessee

MARTIN MARIETTA ENERGY SYSTEMS LIBRARIES
3 4456 0349518 0

INTERNAL DISTRIBUTION

1. C. E. Center
2. Biology Library
3. Health Physics Library
4-5. Central Research Library
6. Reactor Experimental Engineering Library
7-11. Laboratory Records Department
12. Laboratory Records, ORNL R.C.
13. C. E. Larson
14. W. B. Humes (K-25)
15. L. B. Emlet (Y-12)
16. A. M. Weinberg
17. E. H. Taylor
18. E. D. Shipley
19. A. H. Snell
20. F. C. VonderLage
21. R. C. Briant
22. J. A. Swartout
23. S. C. Lind
24. F. L. Culler
25. A. Hollaender
26. J. H. Frye, Jr.
27. W. M. Good
28. M. T. Kelley
29. G. H. Clewett
30. R. S. Livingston
31. K. Z. Morgan
32. T. A. Lincoln
33. A. S. Householder
34. C. P. Keim
35. C. S. Harrill
36. C. E. Winters
37. D. S. Billington
38. D. W. Cardwell
39. E. M. King
40. E. O. Wollan
41. A. J. Miller
42. J. A. Lane
43. R. B. Briggs
44. L. D. Roberts
45. R. N. Lyon
46. W. C. Koehler
47. W. K. Ergen
48. E. P. Blizard
49. M. E. Rose
50. D. D. Cowen
51. R. A. Charpie
52. J. L. Meem
53. C. E. Clifford
54. R. G. Cochran
55. C. L. Storrs
56. L. B. Holland
57. G. M. McCammon
58. F. C. Maienchein
59. E. D. Klema
60. E. B. Johnson
61. J. K. Leslie
62. R. H. Ritchie
63. H. E. Hungerford
64. M. J. Skinner
65. G. C. Williams
66. W. M. Breazeale (consultant)

EXTERNAL DISTRIBUTION

67. D. B. Benedict, C&CCC, South Charleston
68. R. F. Bacher, California Institute of Technology
69. S. V. Manson, Wright Aeronautical Corporation
70. F. T. Bly, Consolidated Vultee Aircraft Corp., Forth Worth
71. G. C. Hanna, Chalk River
72. R. B. Leachman, Los Alamos Scientific Laboratory

73-330. Given distribution as shown in TID-4500 under Physics category

DISTRIBUTION PAGE TO BE REMOVED IF REPORT IS GIVEN PURLIC DISTRIBUTION

TABLE OF CONTENTS

Introduction	1
General Procedure	3
Determination of Fission Rate in "Pinky" Pile	6
Determination of Fission Rate in Special Element	9
Determination of Power in Special Element	17
Energy Released Per Fission	21
Effect of Changes in Pile Constants	25
Corrected Procedure for Determining Reactor Power	25
Acknowledgements	27
Appendix A-- Calibration of Slot 5 of Pinky Pile to Slot 11 of Standard Pile	28
Appendix B - Depression of the Flux in the Uranium Disc	31
Appendix C - Cadmium Ratio of Uranium Disc in Pinky Pile	34
Appendix D - Comparison of Fission Rate in Pinky Pile with that at Midpoint of Special Fuel Element	36
Appendix E - Comparison of Fission Rates at Various Points along Length of Removable Fuel Plate	38
Appendix F - Comparison of the Fission Rate Distribution with the Thermal Flux Distribution	51
Appendix G - Construction and Calibration of Thermocouples	53
Appendix H - Installation and Calibration of Rotómeters	63
Appendix J - Installation of Thermocouples and Water Tubes	66
Appendix K - Data for the Determination of the Power in the Special Element	70
Appendix L - Net Leakage of Radiation into Special Fuel Element	77
References	80

LIST OF FIGURES

Fig. No.		Pg. No.
1	Reactor Loading for Measurement of Energy per Fission; Special Fuel Element in Position 37	4
2	Special Fuel Element	5
3	Comparison of Activation of Fission Catcher Foils in Reactor with Those in Pinky Pile	12
4	Vertical Fission Rate Distribution along the Removable Fuel Plate	14
5	Vertical Neutron Flux Distribution along the Special Fuel Element	16
6	Energy Production in Special Element vs. Reactor Power	20
G-1	Thermocouple Construction	54
G-2	Thermocouple Adapter Assembly for Top of Special Element	57
G-3	Thermocouple Adapter for Bottom of Special Element	58
G-4	Dummy Element Without Insulation or Thermocouple Adapters	61
H-1	Apparatus for Maintaining Constant Water Flow Through Fuel Element	64
J-1	Thermopile Arrangement in Special Element	68

LIST OF TABLES

Table No.		Pg. No.
A-1	Summary of Indium Foil Data (Saturated Activities) in Pinky Pile and Standard Pile	30
C-1	Calculations for Cadmium Ratio of U-Al Sandwich in Slot 5 of Pinky Pile	35
D-1	Determination of Ratio of Fission Rates in Pinky Pile and Special Fuel Element in Reactor	37
E-1	Activity of U-Al Discs at Midposition of Fuel Plate	41
E-2	Activity of Discs Below Center Position of Special Fuel Element in BSR	42
E-3	Activity per Gram of U^{235} in Discs Below Center Position of Special Fuel Element in BSR	43
E-4	Calculated C_3 Activity Values of Discs Below Center Position of Special Fuel Element in BSR -- Data not Normalized	44
E-5	Calculated C_3 Activity Values of Discs Below Center Position of Special Fuel Element in BSR -- Data Normalized by Gold Foils	45
E-6	Activity of Discs Above Center Position of Special Fuel Element in BSR	46
E-7	Activity per Gram of U^{235} in Discs Above Center Position of Special Fuel Element in BSR	47
E-8	Calculated C_3 Activity Values of Discs Above Center Position of Special Fuel Element in BSR -- Data Not Normalized	48
E-9	Calculated C_3 Activity Values of Discs Above Center Position of Special Fuel Element in BSR -- Data Normalized by Gold Foils	49
E-10	Ratios of Fission Rate at Center Position of Fuel Plate to Rates at Other Positions	50

LIST OF TABLES CON'D

Table No.		Pg. No.
F-1	Average of Thermal Flux Measurements on Center Plate and Four Sides of Special Fuel Element	51
F-2	Comparison of Fission Rate with Thermal Flux at Various Positions along Center Fuel Plate	52
H-1	Rotometer Calibrations	65
K-1	Temperature Rise and Water Flow Through Special Fuel Element, Position 37	74
K-2	Temperature Rise and Water Flow Through Elements in Positions 36 and 38 Adjacent to Special Element	75
K-3	Temperature Rise and Water Flow Through Elements in Positions 25, 27, and 47 Adjacent to Special Element	76

Abstract

The energy released per fission was measured in the Bulk Shielding Reactor using a specially constructed fuel element. The special element had a removable center fuel plate from which discs were punched to facilitate measurement of their activation by exposure in the reactor. A similar uranium-bearing disc was activated by exposure in a known neutron flux. By comparison, the actual fission rate in the special fuel element was determined.

The special element was equipped with water tubes at top and bottom through which water was pumped at a known rate. Thermocouples were used to measure the temperature rise across the fuel element, special precautions being taken to prevent heat leakage. The power, or rate of energy production, was determined from the water flow and temperature rise, and a comparison with the fission rate gave the heat released per fission in the special element. The net amount of radiation leaking out of the fuel element (less than 0.2%) was calculated as a correction to this figure.

The energy per fission in the reactor was 193 $\pm$ 5 Mev. The parasitic capture in the Bulk Shielding Reactor is calculated to be 2.7 Mev. Accordingly, the energy released per fission (exclusive of neutrino energy) is 190 $\pm$ 5 Mev.

DETERMINATION OF THE POWER OF THE BULK SHIELDING REACTOR--PART III*

MEASUREMENT OF THE ENERGY RELEASED PER FISSION

J. L. Meem L. B. Holland

G. M. McCammon

Introduction

The power calibration of the Bulk Shielding Reactor from neutron flux measurements has been described in two previous reports(1) hereinafter referred to as Parts I and II. For the calibration gold foils were exposed in various positions throughout the reactor, providing the necessary data to map the thermal neutron flux. The fission rate was then calculated from the known amount of uranium throughout the reactor and the fission cross section. One of the largest uncertainties in this method of determining the power of a reactor rests in the value chosen for the energy released per fission. Accordingly, it was decided to attempt to measure that quantity.

Since the first determination of the BSR power, in which 165 Mev per fission was used, a report by Hanna(2) of Chalk River

---

* In Part I, ORNL-1027, the major title read: Determination of the Power of the Shield Testing Reactor. The term "Bulk Shielding Reactor" has been substituted for "Shield Testing Reactor" in Parts II (ORNL-1438) and III to avoid confusion with the Submarine Thermal Reactor, referred to as the STR.

(1) References are listed at the end of this report.

has appeared in which the best value was chosen as 198 $\pm$ 6 Mev. He evaluated all of the recent work, paying particular attention to the fission fragment velocity measurements done by Leachmen[3] at Los Alamos. According to Hanna's notation, the energy released per fission, E_t, is given by

$$E_t = E_K + E_\beta + E_\gamma + E_n + E_\gamma^*$$

where E_K is the kinetic energy of the fission fragments, $E_\beta + E_\gamma$ is their decay energy (not including neutrino energy), E_n is the kinetic energy of the fission neutrons, and E_γ^* is the prompt gamma-ray energy.

The energy released per fission in a reactor also includes an additional component, E_c, which is the energy liberated in capture processes not leading to fission, viz., nonproductive capture in U^{235}, capture in moderator, capture in reactor structure, etc. Accordingly, a measurement made in a reactor gives E_t', where

$$E_t' = E_t + E_c$$

The various contributions to the total energy per fission in the NRX reactor at Chalk River were estimated[2] as follows:

$$\begin{aligned} E_K &= 168 \pm 5 \text{ Mev} \\ E_\beta + E_\gamma &= 13 \pm 2 \\ E_n &= 5 \pm 0.5 \\ E_\gamma^* &= 4.6 \pm 0.5 \\ E_c &= \underline{7.7 \pm 0.5} \\ E_t' &= 198 \pm 6 \text{ Mev} \end{aligned}$$

Except for some change in the value of E_c because of different materials in the BSR, the various contributions to the total energy should be the same in the BSR as in the NRX.

General Procedure

The reactor was loaded as shown in Fig. 1. A special fuel element was constructed for the experiment and was placed in position 37. This special element (Fig. 2) had a removable center fuel plate from which 1-1/4 in. diameter discs were punched to facilitate measurement of their activation by exposure in the reactor. A similar disc was activated by exposure in a known neutron flux. By comparison, the actual fission rate in the special fuel element could thus be determined.

The special element was equipped with water tubes at top and bottom through which water was pumped at a known rate. Thermocouples were used to measure the temperature rise across the fuel element, special precautions being taken to prevent heat leakage. The power, or rate of energy production, was determined from the water flow and temperature rise, and a comparison with the fission rate gave the heat released per fission in the special fuel element. The net amount of radiation leaking out of the fuel element was calculated as a correction to this figure.

DECLASSIFIED
DWG 17499

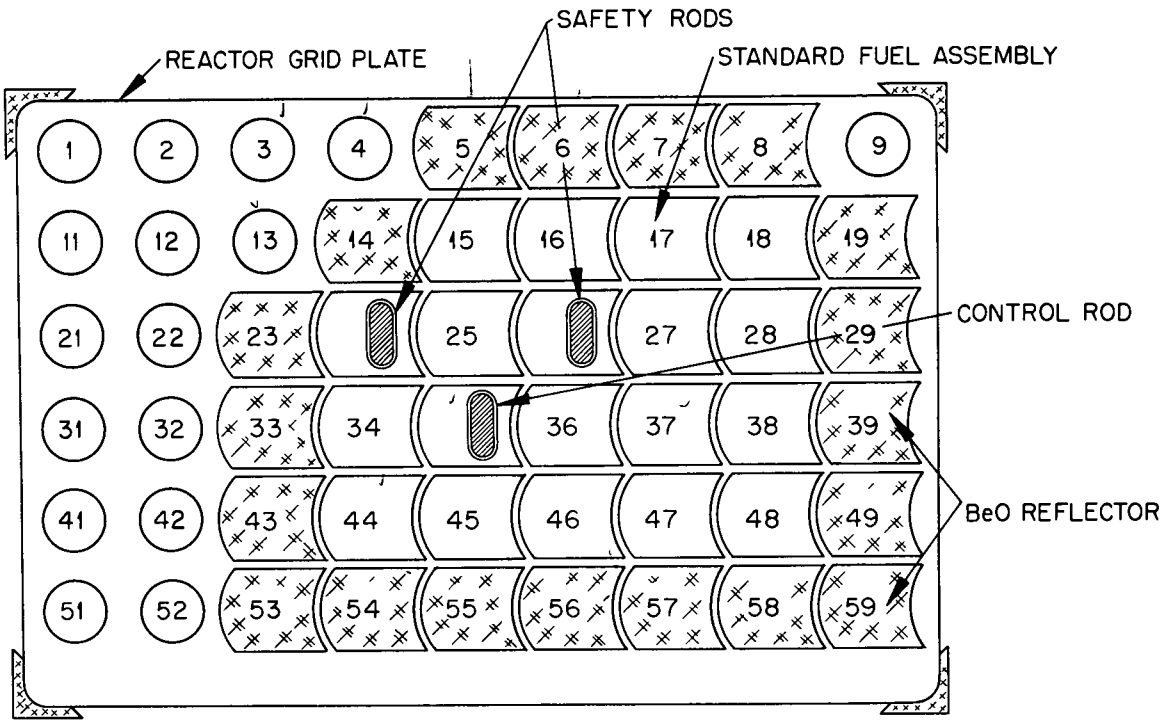

Fig 1 Reactor Loading for Measurement of Energy per Fission, Special Fuel Element in Position 37

DECLASSIFIED Per Letter Instructions Of AEC
SUPERVISOR CENTRAL FILES

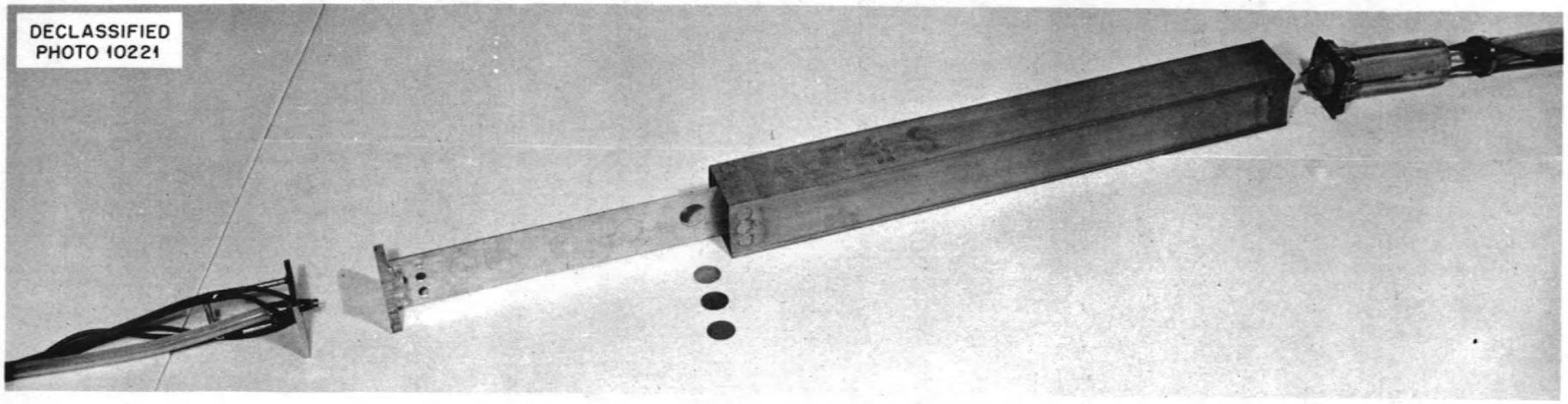

Fig. 2. Special Fuel Element. (Shows Center Fuel Plate, Removable Disks, Thermocouples and Water Tube.)

Determination of Fission Rate in "Pinky" Pile

In order to determine the number of fissions per second in the special fuel element of the BSR, it was first necessary to determine the number of fissions per second in a known flux for use as a standard. The Standard Pile at ORNL had previously been used for this purpose; however, for activation of the fuel-bearing discs a higher flux was required. It was decided to use a polonium-beryllium source placed in a 6 by 6 by 10 ft graphite stack. It then became necessary to calibrate this graphite pile, which will be referred to as the "Pinky" Pile, to the Standard Pile.

Several 25-cm^2 indium foils were exposed at various distances from the source in the Pinky Pile. A point with adequate thermal flux for good counting statistics and low enough resonance activation to enable comparison on the basis of thermal cross sections was desired for exposure of the fuel-bearing discs. The position selected was slot No. 5, which is approximately 54.8 cm above the source. By comparison of the data obtained from exposure of indium foils in this slot with data obtained from similar exposures in a position of known flux[4] in the Standard Pile, the thermal neutron flux of the Pinky Pile was computed to be 3.205×10^4

neutrons/cm^2/sec with a cadmium ratio of 21.76. Details of the measurements are given in Appendix A. It should be noted that the Standard Pile calibration is based on a cross section of gold of 95 barns for 2200-m/sec neutrons.

Knowing the value for the thermal neutron flux in the Pinky Pile, it was then possible to calculate the absolute fission rate in a sample of U^{235} placed in that flux. The sample activated was a specially made disc 1-1/4 in. in diameter which could replace any one of the discs punched from the removable fuel plate. The fuel plate itself (see Fig. 2) had a sandwich-type construction[5,6] consisting of a 20 mil thick uranium-aluminum alloy clad on each side with 20 mil of pure aluminum. The special disc had the same sandwich-type construction; however, for the purpose of counting techniques, as described in the following section, the three layers could be separated as shown in Fig. 2.

The dimensions of the uranium-bearing core of the disc sandwich were:

Thickness	=	0.020 in. (0.0508 cm)
Diameter	=	1.25 in. (3.175 cm)
Area of disc	=	1.228 sq in. (7.92 sq cm)

A chemical analysis of the specially made disc gave 0.1586 g U^{235}.

In the calibration of the Standard Pile (Ref. 4) the gold cross section of 95 barns for a neutron velocity of 2200 m/sec was corrected to 84 barns to correspond to the most probable neutron velocity. Gold has a 1/v cross section and it is assumed that U^{235} has a fission cross section which is very nearly 1/v in this energy region. The fission cross section of 549 barns must be corrected to 485.5 barns to correspond to the most probable neutron velocity in the Pinky Pile. The fission rate in the uranium disc when activated in the given thermal neutron flux of the Pinky Pile could then be calculated:

$$\text{Fissions/sec/g in disc} = 3.205 \times 10^{4} \text{ neutrons/cm}^{2}\text{/sec}$$
$$\times\ 485.5 \times 10^{-24} \text{ cm}^{2}\text{/atom}$$
$$\times\ 0.6023 \times 10^{24} \text{ atoms/mol} \times \frac{1}{235} \text{ mols/g}$$
$$= 3.988 \times 10^{4}$$

This value is the fission rate in the unperturbed neutron flux. The depression of the neutron flux by the absorbing disc was calculated to be 8.44% with the method of Skyrme[7] (see Appendix B). A rough estimate of the flux increase due to the fissions shows this to be entirely negligible.

$$\text{Fissions/sec/g in disc} = (3.988 \times 10^{4}) \times 0.9156$$
$$= 3.651 \times 10^{4} \text{ (corrected value)}$$

Determination of Fission Rate in Special Element

The fission rate in slot 5 of the Pinky Pile having been obtained for use as a standard, it was then possible to determine the fission rate at a particular point in the reactor by comparing the counting rates of a uranium-bearing disc activated in both fluxes. The midpoint of the fuel element was chosen for this determination, after which a comparison method was again used to obtain the variation of flux along the length of the fuel element. With this information the total fission rate in the special element was computed. The procedure is described as follows:

As mentioned previously, several discs 1-1/4 in. in diameter were punched out of the center plate of the special fuel element so that they could be removed and counted after activation. However, for the comparison of the fission rate in the reactor with the fission rate in the Pinky Pile, the specially made disc sandwich with three separable layers replaced the disc punched out at the midpoint of the fuel element center plate. This was necessary for the fission fragment catcher technique used whereby one of the outside aluminum layers was counted. The same fuel disc was used in both the Pinky Pile and the reactor.

The fission fragment catcher method involves counting the radiation of those fission fragments that are captured by the outside aluminum layers. The advantage of this technique is that the background counts due to the natural radioactivity of the uranium are eliminated. In the low neutron flux of the Pinky Pile this background was particularly objectionable.

Since the calculated value of the fission rate (3.651×10^4 fissions/sec/g) for thermal neutrons in the Pinky Pile included a correction for epithermal neutrons, it was necessary to also correct the counting rate of the uranium-bearing disc exposed in the Pinky Pile. This was done through a measurement of the cadmium ratio as described in Appendix C. A correction for the

epithermal neutrons in the reactor was not required, since the power of the reactor is proportional to the fission rate caused by neutrons of all energies.

Ten 10-hr exposures of the specially made uranium disc were made both in slot 5 of the Pinky Pile and at the midpoint of the center plate of the special fuel element in the reactor. A 30-min wait period, after which the induced activity of the aluminum was negligible, was allowed after each exposure. Then 1-min counts were taken at 15-sec intervals for a 60-min period. Plots of the counting rate versus time averaged for the ten exposures in both the Pinky Pile and the reactor are shown in Fig. 3.* (The data for the Pinky Pile is corrected for the cadmium ratio.) Comparing the two curves, it is seen that the fission fragment activity in the Pinky Pile was 0.01599 times that at the midpoint of the special fuel element in the reactor (see Appendix D). Accordingly, the fission rate at the center of the element was established as

$$\frac{3.651 \times 10^4}{0.01599} = 2.283 \times 10^6 \text{ fissions/sec/g}$$

The reactor power for these runs was 0.1 watt (nominal).

Knowing the fission rate at the center of the plate, it was then possible to determine the variation of the fission rate along

* If these curves are plotted on log-log paper a straight line is obtained with a slope of ~ -0.54; see E.P. Blizard, H. E. Stern, and M. K. Hullings, Effective Fission Product Decay Rates for Various Reactor Operation and Shutdown Times, CF-53-8-47 (to be issued).

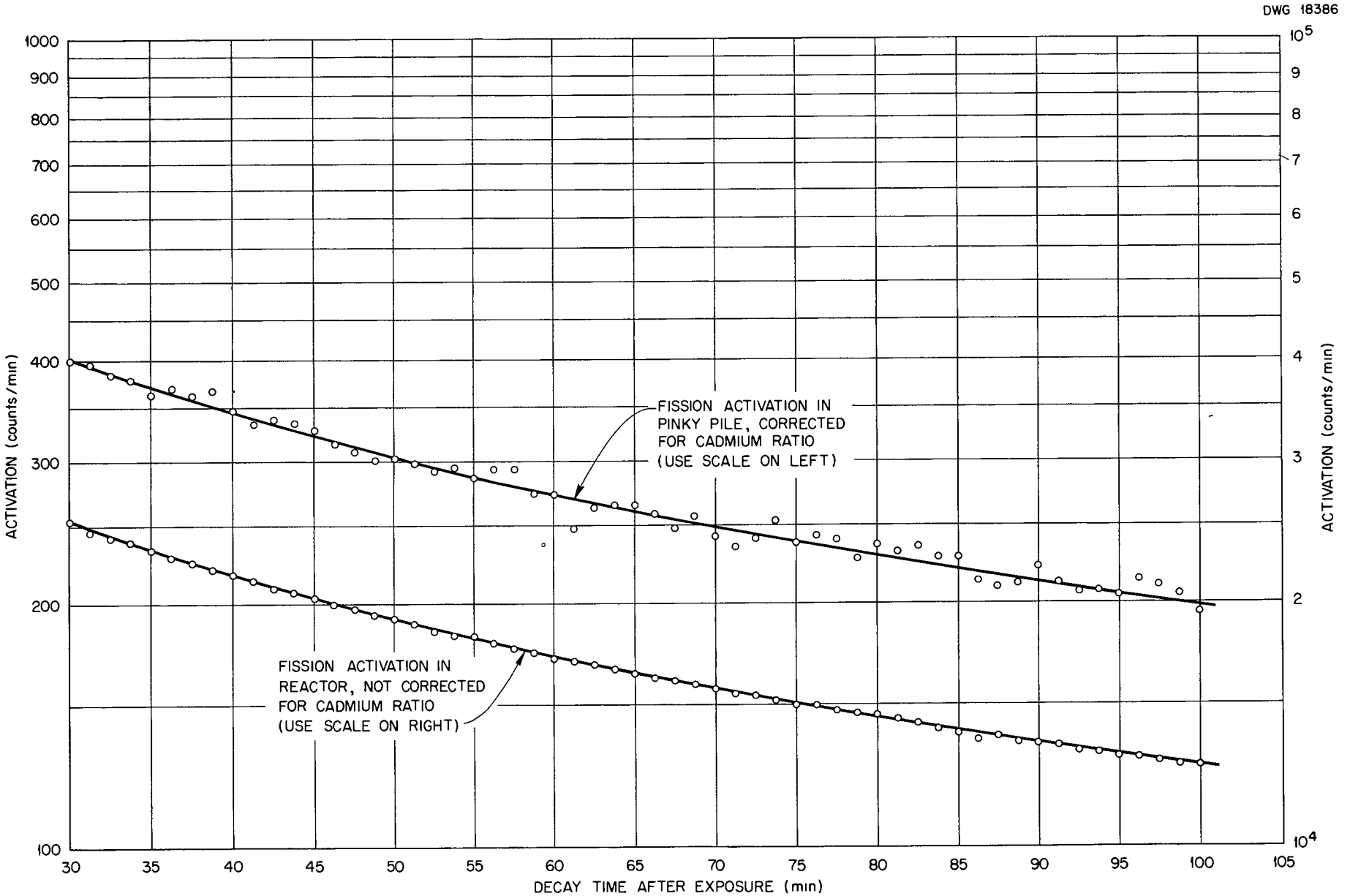

Fig 3 Comparison of Activation of Fission Catcher Foils in Reactor with those in Pinky Pile

the length of the fuel plate. This was done by comparing the counting rate of a disc at the midpoint with the counting rates of discs above and below the midpoint. In this case discs with separable layers were not necessary, since the fission fragment catcher technique was not required. Instead, solid discs were constructed like those punched from the fuel plate. During each run at positions above and below the midpoint, several of these fresh discs replaced some of the discs originally in the plate. These solid discs could be activated sufficiently so that the background from natural activity of the uranium was negligible. The details and results are given in Appendix E.

The ratios of the activation of the discs at various positions along the fuel plate to the activation of the disc at the center position are given in Table E-10 (Appendix E). From these ratios the fission rate distribution along the length of the fuel plate was calculated and plotted as shown in Fig. 4.

As was reported in Part II, gold foil measurements were made along the center fuel plate to determine the thermal neutron flux distribution. A comparison of this flux distribution with the fission rate distribution showed a close correspondence (see Appendix F). Actually, gold foil measurements were also made on

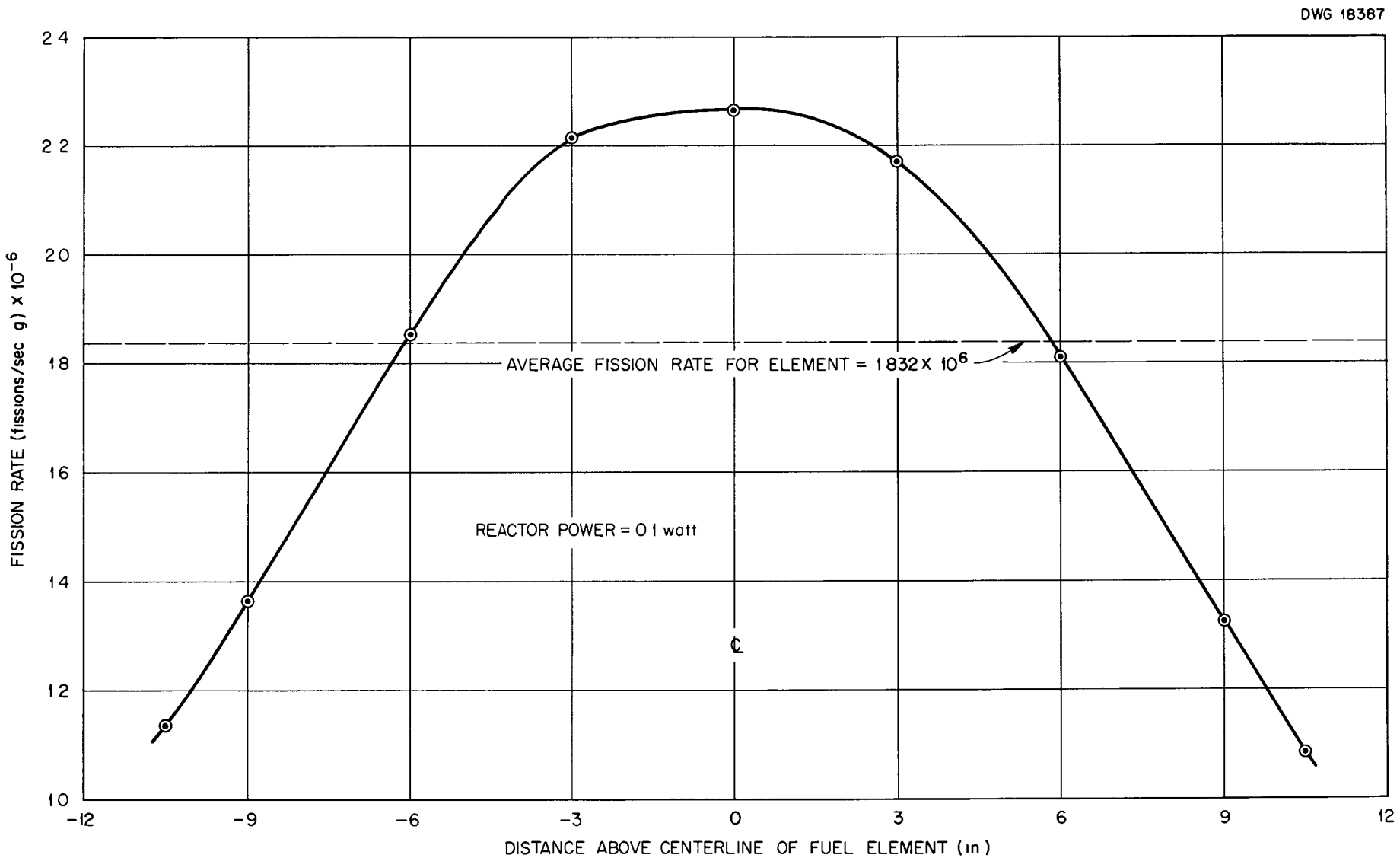

Fig 4 Vertical Fission Rate Distribution Along the Removable Fuel Plate

each side of the special fuel element at positions which corresponded to the measurements on the fuel plate; i.e., for each distance above and below the midpoint there were five points of measurement, the average of which was considered the best value of the thermal flux at that position on the element.

The values of the average fluxes are derived in Appendix F and the flux distribution is shown in Fig. 5. Numerical integration under the curve gave an average flux value of 1.3265×10^6 nv_{th}. As shown in Table F-2 (Appendix F), the average ratio of the fission rate to the thermal flux was 1.381; therefore, the average fission rate in the special element is

$$\text{Fissions/sec/g} = (1.3265 \times 10^6) \times 1.381$$
$$= 1.832 \times 10^6$$

The total weight of fuel in the element being 134.12 g, the total fission rate is then

$$(1.832 \times 10^6) \times 134.12 = 2.457 \times 10^8 \text{ fissions/sec}$$

Since the discs were activated at a reactor power of 0.1 watt (nominal), the fission rate per watt of reactor power in the special element is

$$2.457 \times 10^9 \text{ fissions/sec/watt}$$

DECLASSIFIED Per Letter Instructions Of
SUPERVISOR CENTRAL FILES
ORNL
DECLASSIFIED
DWG 18388

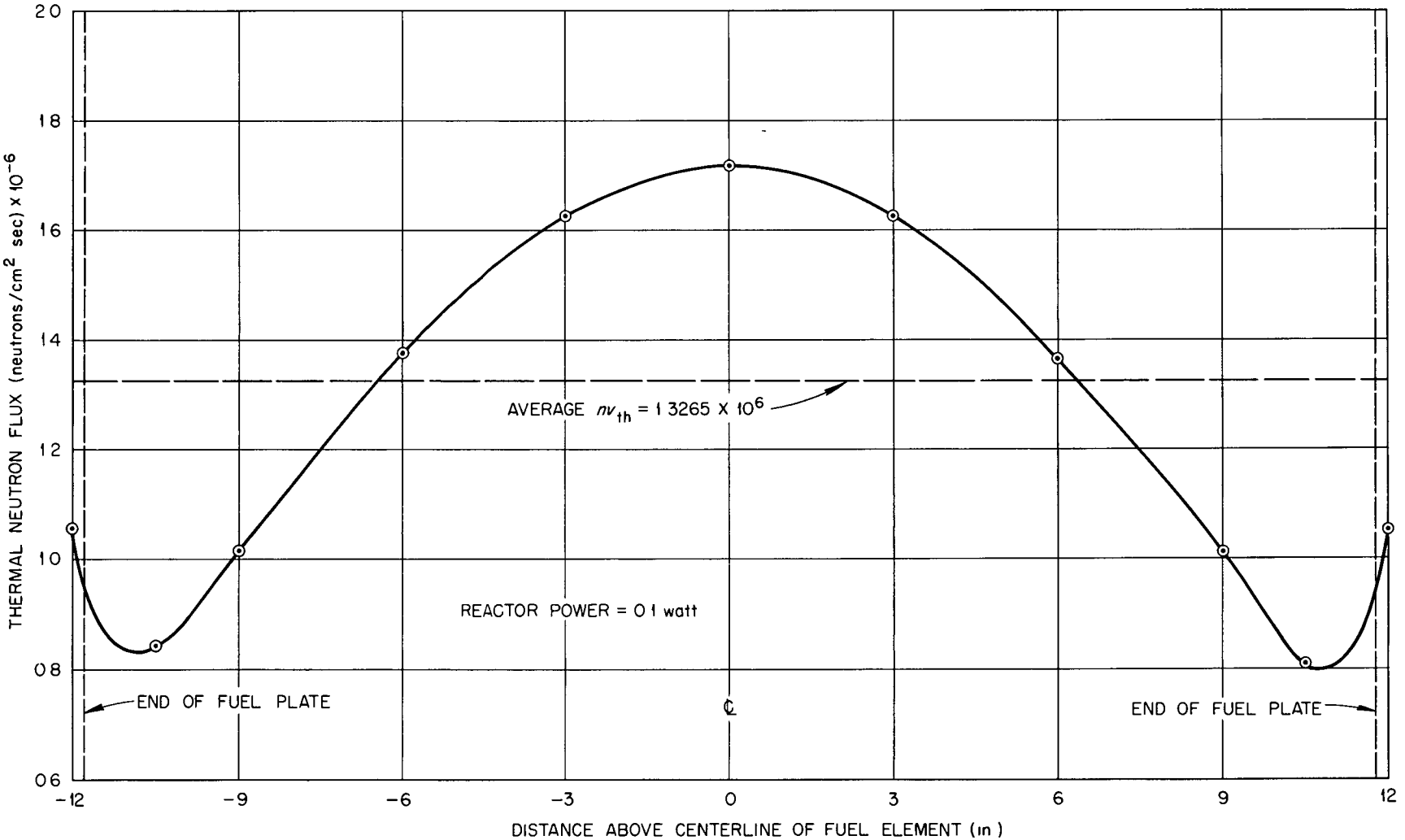

Fig 5 Vertical Neutron Flux Distribution Along the Special Fuel Element

Determination of Power in Special Element

After completion of the fission foil measurements, the special fuel assembly (Fig. 2) was equipped with thermocouples and water flow tubes to measure the temperature rise across the element. With this information and the known water flow and reactor power for each run, the power generated in the special element could be determined. The measurements were made as described below.

The special fuel element was equipped with four thermocouples both at the top and bottom (see Appendixes G and J). By means of an aspirator, water from under the reactor was pulled in at the base of the fuel element and out through the top to a calibrated rotameter (see Appendix H). The four elements surrounding the special element in the reactor lattice (Fig. 1) were also equipped with thermocouples and water flow tubes, and the water flow in each element was varied so that the temperature rise was held as closely as possible to the temperature rise across the special element. In this manner, the heat transfer from the special element to the surrounding elements was minimized

Because of an approximately 1/8-in. space between the special element and each of the four surrounding elements, there was an uncontrolled area of water flow which could cause loss of heat from the special element. This possibility was eliminated by coating

the special element on all four sides with water pump grease, completely filling the openings. This grease also served as insulating material around the element. Previous measurements by gold foils, described in Part II, showed that the substitution of grease for water caused no perturbation of the neutron flux.

At high operating power the fuel elements of the BSR become difficult to handle because of their radioactivity. Consequently, two sets of elements are kept on hand, one "cold" set which is easy to handle as it is never used at high power, and a "hot" set which is used for all high power operation. For the thermocouple runs the reactor was run at powers up to 20 kw, so the "cold" elements which had been used for the fission foil measurements had to be replaced by "hot" elements. The special element was not, however, replaced.

The hot elements chosen had been operated at a high power approximately 6 weeks prior to this installation. Considerable care was taken in changing the elements so as not to disturb the power distribution in the reactor. The reactor was brought to critical after each element was replaced to ensure that the regulating rod position was unperturbed.

Before operation at the higher power level, it was also necessary to reposition the reactor control chambers. In order to

determine the effect of repositioning the control chambers, gold foils were exposed before and after the changes were made. Measurements by an independent fission chamber at a fixed distance from the reactor were also taken before and after the changes. Through these measurements it was found that the reactor power was maintained at 1.095 times the old power for a given setting of the controls. All the power settings for the thermocouple runs were corrected by this amount. (In changing the power of the reactor over a range of 10^5 it was found that the reactor controls were linear to within 1.5% as described in Appendix F of Part II.)

Three runs with the water flow through the special element maintained at 1000, 1500, and 1750 cc/min, respectively, were made to measure the power generated in the element. For each run the reactor power was varied through a range of about 1 to 20 kw, and the temperature rise across the special element was measured. If

W = water flow through the special element (cc/min),

ΔT = temperature rise across the element ($^{\circ}C$),

P = nominal reactor power (kw),

then

$$W \ \Delta T/P = \text{a constant}$$

A plot of $W \ \Delta T/P$ versus P for the three runs is shown in Fig. 6,

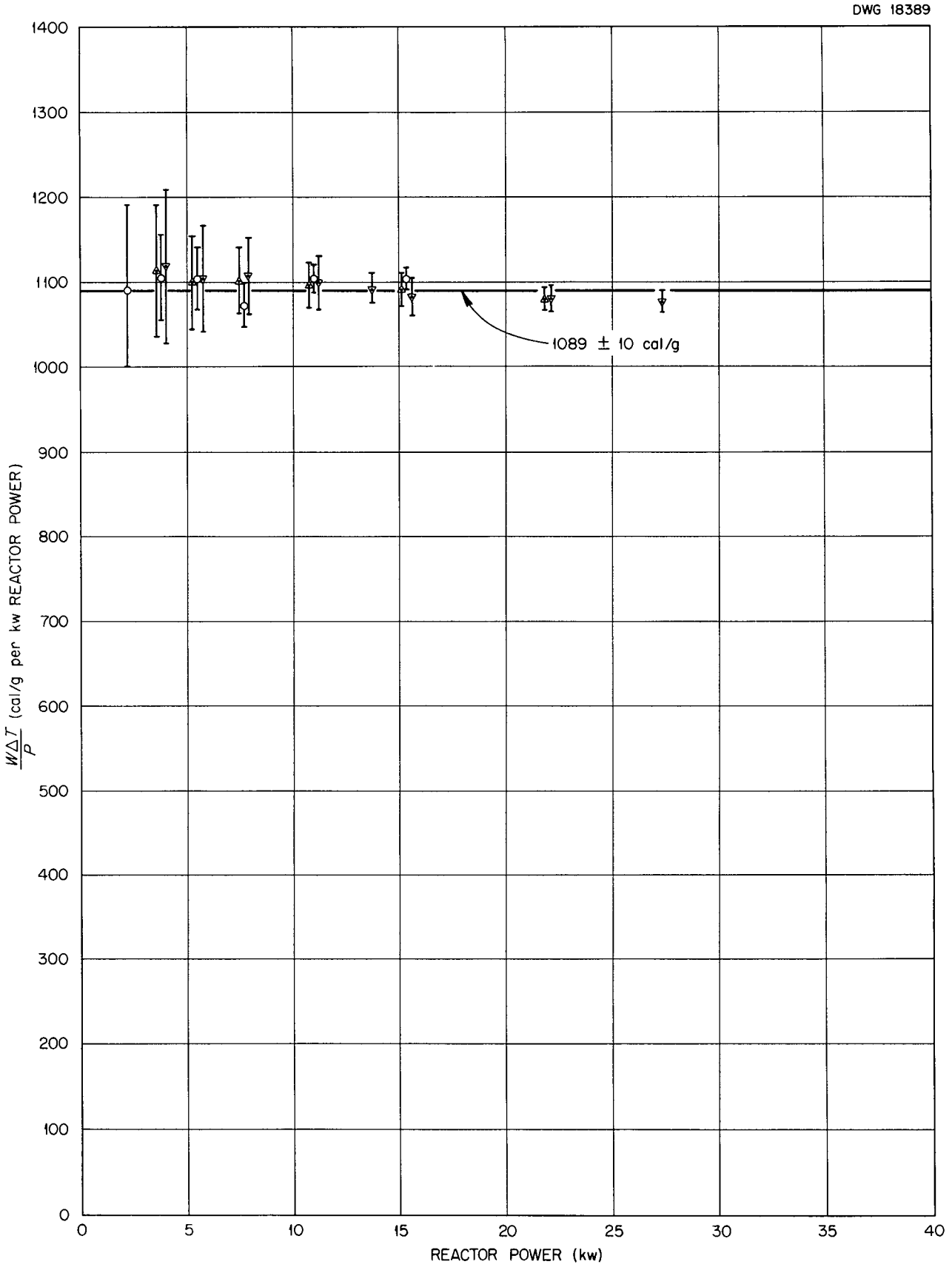

Fig 6 Energy Production in Special Element vs Reactor Power.

and the data is given in Appendix K. The best value found for W $\Delta T/P$ is

$$1089 \text{ cal/min/kw}$$

Multiplying by 4.36×10^8,

$$W \Delta T/P = 4.748 \times 10^{11} \text{ Mev/sec/watt}$$

Energy Released per Fission

Since the power generated in the special element in the BSR was 4.748×10^{11} Mev/sec/watt and the fission rate was 2.457×10^9 fissions/sec/watt, a simple calculation would give the energy released per fission as

$$\frac{4.748 \times 10^{11}}{2.457 \times 10^9} = 193.24 \text{ Mev/fission}$$

However, the leakage of neutrons and gamma rays into or out of the four sides and top and bottom of the special element must be considered. Since the reactor was loaded (see Fig. 1) so that the average power of the surrounding elements was approximately the same as that of the special element, the net radiation leakage in or out of the special element was expected to be small but not necessarily negligible. With an approximate method the net leakage

was calculated as 0.17% into the element (see Appendix L); i.e.,

$$\text{Leakage} = 193.24 \times 0.0017 = 0.34 \text{ Mev/fission}$$

If this leakage is subtracted, the best rounded off value for the experiment is then

193 Mev/fission

Before the above value can be accepted as final, three possible experimental errors must be explained:

(1) Activation of Fission Foils in Pinky Pile. As is discussed in Appendix D, the counting rates of the fission catcher foils exposed in the Pinky Pile were much less than those of the foils exposed in the reactor, resulting in an appreciable statistical error. An evaluation by the ORNL Mathematics Panel indicated a possible error of $\pm 1.5\%$ in the ratio (0.01599) of the activity in the Pinky Pile to the activity in the reactor.

(2) Extrapolation of Pile Power. Since the fission foils were exposed in the reactor at a power of 0.1 watt and the thermocouple runs were made at 1 to 20 kw, the linearity of the reactor controls over a range of 10^5 in power must be considered. In Appendix F of Part II it was shown that the

controls are linear within $\pm 1.5\%$.

(3) Sensitivity of Thermocouples. The EMF of the thermocouples could be read to a value corresponding to $\pm 0.2^{\circ}C$. As is discussed in Appendix K, this limiting sensitivity fixed the accuracy of the measurement of the heat generated in the special element to $\pm 1\%$.

Since these errors are completely independent, they may be combined as the square root of the sum of the squares to give a calculated error of $\pm 2.15\%$. The absolute error is then ± 4.2 Mev. If allowance is made for small unknown errors, the over-all probable error for the experiment is estimated as ± 5 Mev.

The value of 193 ± 5 Mev from this experiment differs from Hanna's value of 198 ± 6 Mev by 5 Mev. This difference is due to the neutron capture term E_c, which Hanna calculated to be 7.7 Mev in the NRX (see Introduction and Ref. 2). He estimated that in the NRX for every slow neutron producing fission in U^{235} there were (1) 0.18 neutrons captured in U^{235}, (2) 0.84 neutrons captured in U^{238}, and (3) 0.22 neutrons captured in other substances.

The composition of the BSR is 0.2% uranium, 41.5% aluminum, and 58.3% water. Using the appropriate thermal capture cross

sections, it is estimated for every slow neutron producing fission in the BSR there are (1) 0.18 neutrons captured in U^{235}, (2) 0.10 neutrons captured in Al, and (3) 0.24 neutrons captured in water. The capture in U^{238} is negligible.

Again following Hanna, it is possible to determine the sum of these contributions as follows:

(1) The neutron binding energy in U^{235} is estimated as 6.8 Mev; then

$$6.8 \times 0.18 = 1.2 \text{ Mev}$$

(2) A capture gamma-ray energy of 7 Mev is assumed in Al with a decay energy of 3.7 Mev; then

$$10.7 \times 0.10 = 1.1 \text{ Mev}$$

(3) A capture in water is accompanied by the well-known 2.2-Mev gamma with no decay; then

$$2.2 \times 0.24 = 0.5 \text{ Mev}$$

Total 2.8 Mev

Hanna assumed a value of 1.035 for the fast fission factor in the NRX, a value which is probably correct for the BSR also. Accordingly,

$$E_c = \frac{2.8}{1.035} = 2.7 \text{ Mev}$$

The quantity E_c can be calculated for any reactor; therefore,

$$E_t' = (190 + E_c) \pm 5 \text{ Mev}$$

Effect of Changes in Pile Constants

The value of the energy per fission as determined by this experiment was based on a thermal capture cross section of gold of 95 barns and a thermal fission cross section of U^{235} of 549 barns. If these values are revised, the effect of these changes can be calculated from the general formulas:

$$E_t = 190 \times \frac{\sigma_{Au}}{95} \times \frac{549}{\sigma_f}$$

and

$$E_t' = E_t + E_c$$

Corrected Procedure for Determining Reactor Power

As mentioned in the introduction, the largest uncertainty in the determination of the BSR power from thermal neutron flux

measurements was in the value of the energy released per fission. The correct procedure can now be summarized as follows:

Let

P = power (watts),

G = weight of U^{235} (g).

Since

$$\text{fissions/sec} = 1.381 \times nv_{th} \times G$$

then

$$P = (1.381 \times nv_{th} \times G) \text{ fissions/sec} \times 193 \text{ Mev/fission} \times 1.60 \times 10^{-13} \text{ joules/Mev}$$

or

$$P = (4.264 \times 10^{-11} \times nv_{th} \times G) \text{ watts}$$

For example, consider the special fuel element in this experiment. At a nominal reactor power of 1 watt, the average thermal neutron flux was 1.3265×10^{7} and the weight of the fuel was 134.12 g. Therefore, the power in the special element was

$$P' = (4.264 \times 10^{-11})\ (1.3265 \times 10^{7})\ (134.12)$$
$$= 7.586 \times 10^{-2} \text{ watts}$$

This can be checked against the temperature measurements in the

special element, where

$$W\ \Delta T/P = 4.748 \times 10^{11}\ \text{Mev/sec} \qquad \text{(for 1-watt nominal power)}$$

or

$$P' = (4.748 \times 10^{11}\ \text{Mev/sec})\ (1.60 \times 10^{-13}\ \text{joules/Mev})$$
$$= 7.597 \times 10^{-2}\ \text{watts}$$

This value of P' is slightly higher because the small leakage of radiation into the special element was included in the measurement of $W\ \Delta T/P$.

Acknowledgements

Many individuals contributed to the success of this experiment. In particular, thanks are due to Mrs. Elizabeth Johnson for her help in taking the foil data and to Mr. James K. Leslie for his assistance in handling the reactor. Mr. S. V. Manson, NACA, Cleveland, Ohio, was of considerable assistance in devising means for minimizing the heat leakage, and Mr. Frank T. Bly, Convair, Fort Worth, Texas, contributed to the method of determining the fission rate. Many helpful discussions were held with Dr. E. D. Klema and Mr. R. H. Ritchie on the general method of performing the experiment.

Appendix A

CALIBRATION OF SLOT 5 OF PINKY PILE TO SLOT 11 OF STANDARD PILE

A series of exposures were made with large indium foils (6.25 by 4.0 cm) in slot 5 of the Pinky Pile, which contained an approximately 30-curie polonium-beryllium source. Bare and cadmium-covered foil exposures were made and each foil was counted several times. The results from the counts were averaged for each condition of exposure and a saturated activity was therefore determined for both bare and cadmium-covered foils (see Table A-1). All exposures were corrected for the decay of the source. Likewise, a set of exposures on indium foils were made in slot 11 of the Standard Pile in which position the thermal neutron flux had been accurately determined.[4] The following data was obtained from the indium foils in slot 5 of the Pinky Pile.

Distance from the source	=	54.82 cm
Bare saturated activity	=	5.448×10^5 counts/min
Cadmium-covered saturated activity	=	2.504×10^4 counts/min
Thermal saturated activity	=	5.198×10^5 counts/min
Cadmium ratio	=	21.76
Thermal neutron flux	=	3.205×10^4 nv_{th}

The thermal flux in slot 5 of the Pinky Pile determined on the basis of activity in slot 11 of the Standard Pile was calculated as follows:

$$nv_{th} \text{ in slot } 5 = \frac{A_s^{th} \text{ in slot } 5}{A_s^{th} \text{ in slot } 11} \times nv_{th} \text{ of slot } 11$$

where

nv_{th} = thermal neutron flux,

A_s^{th} = thermal saturated activity.

Since

nv_{th} in slot 11 = 703,

A_s^{th} in slot 11 = 1.140×10^4,

A_s^{th} in slot 5 = 5.198×10^5,

then

$$nv_{th} \text{ in slot } 5 = \frac{5.198 \times 10^5}{1.140 \times 10^4} \times 703$$

$$= 3.205 \times 10^4 \text{ disintegrations/sec/cm}^2$$

It should be noted that the Standard Pile calibration is based on a cross section of gold of 95 barns for 2200-m/sec neutrons.

Table A-1. Summary of Indium Foil Data (Saturated Activities) in Pinky Pile and Standard Pile

Bare Foil Exposure			Cadmium-Covered Foil Exposure		
	(counts/min)			(counts/min)	
Run No.	A_s(top)[a]	A_s(back)	Run No.	A_s(top)	A_s(back)
Slot 5 of Pinky Pile					
1	5.474×10^5	5.468×10^5	1	2.656×10^4	2.402×10^4
	5.519×10^5	5.414×10^5		2.621×10^4	2.420×10^4
	5.391×10^5	5.423×10^5		2.592×10^4	2.373×10^4
	5.436×10^5	5.391×10^5		2.632×10^4	2.396×10^4
2	5.523×10^5	5.433×10^5	2	2.640×10^4	2.382×10^4
	5.505×10^5	5.428×10^5		2.633×10^4	2.369×10^4
	5.421×10^5	5.418×10^5		2.638×10^4	2.358×10^4
	5.439×10^5	5.412×10^5		2.565×10^4	2.399×10^4
3	5.507×10^5	5.453×10^5	3	2.622×10^4	2.421×10^4
	5.480×10^5	5.499×10^5		2.627×10^4	2.388×10^4
	5.474×10^5	5.383×10^5		2.585×10^4	2.370×10^4
	5.490×10^5	5.380×10^5		2.643×10^4	2.361×10^4
Avg.	5.448×10^5		Avg.	2.504×10^4	
Slot 11 in Standard Pile					
1	1.142×10^4	1.147×10^4	No appreciable count on cadmium-covered foil		
	1.163×10^4	1.131×10^4			
	1.154×10^4	1.139×10^4			
2	1.129×10^4	1.147×10^4			
	1.155×10^4	1.129×10^4			
	1.132×10^4	1.137×10^4			
	1.129×10^4	1.140×10^4			
3	1.143×10^4	1.128×10^4			
	1.150×10^4	1.150×10^4			
	1.147×10^4	1.140×10^4			
	1.121×10^4	1.131×10^4			
Avg.	1.140×10^4				

(a) Saturated activity, top side of foil.

Appendix B

DEPRESSION OF THE FLUX IN THE URANIUM DISC

According to Skyrme,[7] the rate of neutron capture in an absorbing disc may be expressed as:

$$\pi a^2 \, nv \, t \left\{ 1 - t \left[\frac{1}{2} E(t) + A(g) + D_1 - D_1' \right] \right\}$$

where

nv = neutron flux,

a = radius of disc,

t = $T\alpha'$ (T = thickness of the disc; α' = inverse mean free path)

and the terms $E(t)$, $A(g)$, D_1, and D_1' are constants as described by Skyrme. The perturbation of the flux by the uranium disc is:

$$t \left[\frac{1}{2} E(t) + A(g) + D_1 - D_1' \right]$$

The specially made disc, containing a U-Al core sandwiched between two pure aluminum layers,* was exposed in graphite (the "Pinky" Pile) as described in the text. For these calculations the effect of the aluminum was neglected and it was assumed that a uranium disc was placed in a graphite medium.

---

*This disc is described in detail on p. 7.

The density of uranium in the disc was 0.394 g/cc. Using an absorption cross section of 645 barns for U^{235}, the inverse mean free path is

$$\alpha' = 0.651 \text{ cm}^{-1}$$

Since T = 0.0508 cm,

$$t = 0.0331$$

The quantity, g, is defined as

$$g = a\alpha'$$

where a is the radius of the disc. Since a = 1.59,

$$g = 1.035$$

Knowing g and t and using Fig. (ii) from the appendix of Ref. (7), the quantity

$$\frac{1}{2}E(t) + A(g) = 2.15$$

D is evaluated from the relationship

$$D_1 = \frac{4}{\pi} \frac{a}{\lambda} \left(1 - \frac{3\pi}{16} \frac{a}{L}\right)$$

where λ and L are the mean free path and diffusion length in graphite.

Using

$\lambda = 2.5$ cm,

$L = 50$ cm,

then

$$D_1 = 0.794$$

Following Ref. (7),

$$D_1' = 0.09$$

Therefore, the perturbation

$$t\left(\frac{1}{2} E(t) + A(g) + D_1 - D_1'\right) = 0.0844$$

The data must be corrected by 8.44%.

Appendix C

CADMIUM RATIO OF URANIUM DISC IN PINKY PILE

To determine the thermal activity on the U-Al sandwich* which was exposed in slot 5 of the Pinky Pile, it was necessary to find the cadmium ratio on the disc. This was done by making ten 10-hr runs on the bare sandwich and likewise on a cadmium-covered sandwich. A 30-min decay period was allowed after each run before the disc was counted; a continuous count was then made for 60 min. For each condition of exposure an average count per minute was determined, from which the cadmium ratio and the percentage of total activity due to thermal neutrons were computed. It was found that 96.22% of the total activity was due to thermal activity, and this value was applied to all bare data taken on the U-Al sandwich in the Pinky Pile. A summary of the data is shown in Table C-1.

---

* This disc is described in detail on p. 7.

Table C-1. Calculations for Cadmium Ratio of U-Al Sandwich in Slot 5 of Pinky Pile

Bare Sandwich Exposure		Cadmium-Covered Sandwich Exposure	
Run No.	(counts/min)	Run No.	(counts/min)
1	300.3	1	2.154
2	324.3	2	16.82
3	273.5	3	24.51
4	305.3	4	11.26
5	293.8	5	11.70
6	321.4	6	9.915
7	286.2	7	9.597
8	310.5	8	11.70
9	268.4	9	12.41
10	295.4	10	2.482
Avg.	297.9	Avg.	11.25

$$\text{Cadmium ratio} = \frac{\text{Total activity}}{\text{Cadmium activity}} = 26.48$$

Cadmium activity = 3.776% of total activity

Thermal activity = 96.22% of total activity

Appendix D

COMPARISION OF FISSION RATE IN PINKY PILE WITH THAT AT MIDPOINT OF SPECIAL FUEL ASSEMBLY

In order to compare the fission rate of slot 5 in the Pinky Pile to that at the midpoint of the special fuel assembly in the reactor, it was first necessary to determine accurately the activity at each position. This was done by exposing a specially made disc* containing a U-Al core sandwiched between two pure aluminum layers and using the fission fragment catcher technique. Ten 10-hr exposures were made in both locations. After a 30-min wait period, 1-min counts of the activity in the aluminum catcher foils were recorded at 15-sec intervals for a period of 60 min. The activity was much higher in the reactor than in the Pinky Pile, and consequently the statistics were much better.

An accurate ratio of the two positions was established from the first 10 counts on the foil exposures in each location. This ratio of the fission rate in the Pinky Pile to that at the midpoint of the special element in the reactor was found to be 0.01599 with a precision of $\pm 1.5\%$. The data is given in Table D-1 in which the Pinky Pile activities are corrected for the uranium-cadmium ratio.

---

* This disc is described in detail on p. 7.

Table D-1. Determination of Ratio of Fission Rates in Pinky Pile and Special Fuel Element in Reactor

Decay Time (min)	Average Thermal Activity (counts/min)		Ratio
	Slot 5 of Pinky Pile[a]	Midpoint of Special Fuel Element in Reactor	
30	399.5	25270	0.01581
31 1/4	395.8	24545	0.01612
32 1/2	382.7	24139	0.01585
33 3/4	377.1	23825	0.01583
35	362.4	23266	0.01558
36 1/4	370.1	22807	0.01623
37 1/2	362.0	22456	0.01612
38 3/4	367.7	22018	0.01670
40	347.7	21730	0.01600
41 1/4	333.9	21323	0.01566
Avg.			0.01599

(a) Corrected for cadmium ratio.

Appendix E

COMPARISION OF FISSION RATES AT VARIOUS POINTS ALONG LENGTH OF REMOVABLE FUEL PLATE

The fission rate at the center of the removable plate of the special element having been established, it was possible to determine the variation of the fission rate along the length of the plate. This could be carried out by comparing the activations of U-Al discs exposed at different positions on the plate with the activation of a disc at the midpoint.

For these measurements it was not necessary to use specially made discs with separable layers since the fission fragment catcher technique was not required. Instead, solid fuel discs were constructed like those punched from the plate. During each run these discs replaced the discs originally in the plate at those positions where measurements were desired. After activation the discs were counted with an end-window G-M tube. In the reactor the activation induced by fission was high enough to make negligible the natural radioactivity of the uranium.

All runs were made in hole 37 of the BSR and were of 2 hr duration at a nominal reactor power of 0.5 watt. After a 30-min

wait period, five 10-min counts at 5-min intervals were made on each run. The counting periods were designated as C_1, C_2, C_3, C_4 and C_5.

During the first three runs discs were exposed at the midpoint of the plate. After each run the activity of the disc during each of the five counting periods was obtained, and the average ratio of the counting rate during period C_3 to each of the other periods was thus established (see Table E-1).

Measurements were then made to determine the relative activities at various positions on the plate. New discs were placed in positions 3, 6, 9, and 10-1/2 in. below the midpoint during each of the next four runs. A new disc was also placed at the midpoint during each run to verify previous activation measurements at that point. (At the same time gold foils were exposed at a fixed position in the reactor as a basis for normalizing the data.) The sequence in which the discs were counted was changed for every run; thus, when the four runs had been completed one disc had been counted during each of the four periods C_1, C_2, C_4, and C_5 for every position on the plate (see Table E-2). The disc placed at the midpoint was always counted during the C_3 period. The activities per gram of U^{235} were obtained by dividing each activity from the various runs by the

absolute amount of U^{235} in the disc as determined by chemical analysis (see Table E-3).

In order to determine what the activities per gram would have been had they all been counted during the C_3 period, the ratios of the counting periods found on the midposition (Table E-1) were applied and for each position below the midpoint four C_3 values were obtained (see Table E-4). These values were then normalized by use of the gold foil data (see Table E-5).

Similar runs were made with new discs placed in positions 3, 6, 9, and 10-1/2 in. above the midposition. The data are given in Tables E-6 through E-9.

An average value of the counting rate for each position above and below the center point of the fuel plate thus determined, the ratios of the fission rate at the midposition to the other positions were computed. The corresponding actual fission rates (2.283×10^6 fissions/sec/g at the midpoint) were then determined. Both the ratios and the fission rates are given in Table E-10. A plot of the fission rate distribution is shown in Fig. 5 of the text.

Table E-1. Activity of U-Al Discs at Midposition of Fuel Plate

Counting Period	Activity (counts/10 min)				Ratio of C_3 to Counting Period
	Run 1	Run 2	Run 3	Avg.	
C_1	4.3409×10^4	4.2082×10^4	4.3889×10^4	4.3127×10^4	0.6024
C_2	3.2427×10^4	3.1789×10^4	3.3184×10^4	3.2467×10^4	0.8001
C_3	2.5960×10^4	2.5432×10^4	2.6542×10^4	2.5978×10^4	1.0000
C_4	2.1665×10^4	2.1260×10^4	2.2333×10^4	2.1753×10^4	1.1942
C_5	1.8535×10^4	1.7965×10^4	1.9064×10^4	1.8521×10^4	1.4026

Table E-2. Activity of Discs Below Center Position of Special Fuel Element in BSR

Run No.	Disc No.	Counting Period	Activity (counts/10 min)				
			At ℄	3 in. Below	6 in. Below	9 in. Below	10-1/2 in. Below
4U	14	C_1		4.067×10^4			
	15	C_2			2.608×10^4		
	13	C_3	2.638×10^4				
	17	C_4				1.279×10^4	
	18	C_5					9.169×10^3
5U	23	C_1					2.179×10^4
	20	C_2		3.160×10^4			
	19	C_3	2.611×10^4				
	21	C_4			1.720×10^4		
	25	C_5				1.113×10^4	
6U	27	C_1				2.680×10^4	
	28	C_2					1.594×10^4
	26	C_3	2.669×10^4				
	29	C_4		2.121×10^4			
	30	C_5			1.502×10^4		
7U	34	C_1			3.516×10^4		
	35	C_2				1.912×10^4	
	31	C_3	2.586×10^4				
	33	C_4					1.080×10^4
	32	C_5		1.787×10^4			

Table E-3. Activity per Gram of U^{235} in Discs Below Center Position of Special Fuel Element in BSR

Run No.	Disc. No.	Counting Period	Total U (g)	Activity (counts/10 min/g)				
				At ℄	3 in. Below	6 in. Below	9 in. Below	10 1/2 in. Below
4U	14	C_1	0.1527		2.663×10^5			
	15	C_2	0.1552			1.681×10^5		
	13	C_3	0.1588	1.661×10^5				
	17	C_4	0.1545				8.276×10^4	
	18	C_5	0.1543					5.942×10^4
5U	23	C_1	0.1564					1.393×10^5
	20	C_2	0.1555		2.032×10^5			
	19	C_3	0.1538	1.698×10^5				
	21	C_4	0.1533			1.220×10^5		
	25	C_5	0.1557				7.150×10^4	
6U	27	C_1	0.1596				1.679×10^5	
	28	C_2	0.1549					1.029×10^5
	26	C_3	0.1544	1.729×10^5				
	29	C_4	0.1551		1.368×10^5			
	30	C_5	0.1533			9.798×10^4		
7U	34	C_1	0.1544			2.277×10^5		
	35	C_2	0.1542				1.240×10^5	
	31	C_3	0.1540	1.588×10^5				
	33	C_4	0.1555					6.947×10^4
	32	C_5	0.1537		1.163×10^5			

Table E-4. Calculated C_3 Activity Values of Discs Below Center Position of Special Fuel Element in BSR -- Data Not Normalized

Run No.	Counting Period	C_3 Activity Values (counts/10 min/g)			
		3 in. Below	6 in. Below	9 in. Below	10-1/2 in. Below
4U	C_1	1.604×10^5			
	C_2		1.345×10^5		
	C_4			9.883×10^4	
	C_5				8.334×10^4
5U	C_1				8.395×10^4
	C_2	1.626×10^5			
	C_4		1.340×10^5		
	C_5			1.003×10^5	
6U	C_1			1.011×10^5	
	C_2				8.234×10^4
	C_4	1.633×10^5			
	C_5		1.374×10^5		
7U	C_1		1.372×10^5		
	C_2			9.920×10^4	
	C_4				8.296×10^4
	C_5	1.631×10^5			
Avg.		1.624×10^5	1.358×10^5	9.986×10^4	8.315×10^4

Table E-5. Calculated C_3 Activity Values of Discs Below Center Position of Special Fuel Element in BSR -- Data Normalized by Gold Foils

Run No.	Counting Period	C_3 Activity Values (counts/10 min/g)			
		3 in. Below	6 in. Below	9 in. Below	10-1/2 in. Below
4U	C_1	1.616×10^5			
	C_2		1.354×10^5		
	C_4			9.952×10^4	
	C_5				8.393×10^4
5U	C_1				8.382×10^4
	C_2	1.624×10^5			
	C_4		1.338×10^5		
	C_5			1.001×10^5	
6U	C_1			1.005×10^5	
	C_2				8.184×10^4
	C_4	1.623×10^5			
	C_5		1.366×10^5		
7U	C_1		1.362×10^5		
	C_2			9.851×10^4	
	C_4				8.238×10^4
	C_5	1.619×10^5			
Avg.		1.6205×10^5	1.355×10^5	9.966×10^4	8.299×10^4

Table E-6. Activity of Discs Above Center Position of Special Fuel Element in BSR

Run No.	Disc. No.	Counting Period	Activity (counts/10 min)				
			At ℄	3 in. Above	6 in. Above	9 in. Above	10-1/2 in. Above
8U	37	C_1		4.079×10^4			
	38	C_2			2.567×10^4		
	36	C_3	2.627×10^4				
	39	C_4				1.266×10^4	
	40	C_5					8.879×10^3
9U	41	C_1					2.021×10^4
	43	C_2		3.100×10^4			
	45	C_3	2.596×10^4				
	42	C_4			1.761×10^4		
	44	C_5				1.054×10^4	
10U	49	C_1				2.494×10^4	
	50	C_2					1.533×10^4
	46	C_3	2.582×10^4				
	47	C_4		2.078×10^4			
	48	C_5			1.458×10^4		
11U	53	C_1			3.472×10^4		
	54	C_2				1.841×10^4	
	51	C_3	2.568×10^4				
	55	C_4					1.024×10^4
	52	C_5		1.804×10^4			

Table E-7. Activity per Gram of U^{235} in Discs Above Center Position of Special Fuel Element in BSR

Run No.	Disc. No.	Counting Period	Total U (g)	Activity (counts/10 min/g)				
				At ℄	3 in. Above	6 in. Above	9 in. Above	10-1/2 in. Above
8U	37	C_1	0.1550		2.632×10^5			
	38	C_2	0.1553			1.653×10^5		
	36	C_3	0.1513	1.736×10^5				
	39	C_4	0.1534				8.254×10^4	
	40	C_5	0.1550					5.728×10^4
9U	41	C_1	0.1542					1.311×10^5
	43	C_2	0.1563		1.983×10^5			
	45	C_3	0.1607	1.616×10^5				
	42	C_4	0.1529			1.152×10^5		
	44	C_5	0.1547				6.814×10^4	
10U	49	C_1	0.1521				1.639×10^5	
	50	C_2	0.1563					9.810×10^4
	46	C_3	0.1626	1.588×10^5				
	47	C_4	0.1563		1.329×10^5			
	48	C_5	0.1602			9.099×10^4		
11U	53	C_1	0.1587			2.188×10^5		
	54	C_2	0.1554				1.185×10^5	
	51	C_3	0.1549	1.658×10^5				
	55	C_4	0.1543					6.636×10^4
	52	C_5	0.1595		1.131×10^5			

Table E-8. Calculated C_3 Activity Values of Discs Above Center Position of Special Fuel Element in BSR -- Data not Normalized

Run No.	Counting Period	C_3 Activity Values (counts/10 min/g)			
		3 in. Above	6 in. Above	9 in. Above	10-1/2 in. Above
8U	C_1	1.585×10^5			
	C_2		1.322×10^5		
	C_4			9.857×10^4	
	C_5				8.035×10^4
9U	C_1				7.896×10^4
	C_2	1.587×10^5			
	C_4		1.376×10^5		
	C_5			9.558×10^4	
10U	C_1			9.876×10^4	
	C_2				7.849×10^4
	C_4	1.588×10^5			
	C_5		1.276×10^5		
11U	C_1		1.318×10^5		
	C_2			9.480×10^4	
	C_4				7.924×10^4
	C_5	1.586×10^5			
Avg.		1.5865×10^5	1.323×10^5	9.693×10^4	7.926×10^4

Table E-9. Calculated C_3 Activity Values of Discs Above Center Position of Special Fuel Element in BSR-- Data Normalized by Gold Foils

Run No.	Counting Period	C_3 Activity Values (counts/10 min/g)			
		3 in. Above	6 in. Above	9 in. Above	10-1/2 in. Above
8U	C_1	1.595×10^5			
	C_2		1.330×10^5		
	C_4			9.916×10^4	
	C_5				8.083×10^4
9U	C_1				7.931×10^4
	C_2	1.594×10^5			
	C_4		1.382×10^5		
	C_5			9.601×10^4	
10U	C_1			9.717×10^4	
	C_2				7.724×10^4
	C_4	1.562×10^5			
	C_5		1.256×10^5		
11U	C_1		1.326×10^5		
	C_2			9.537×10^4	
	C_4				7.971×10^4
	C_5	1.596×10^5			
Avg.		1.587×10^5	1.324×10^5	9.693×10^4	7.927×10^4

Table E-10. Ratios of Fission Rate at Center Position of Fuel Plate to Rates at Other Positions

Position on Special Fuel Element	Ratio	Calculated Fission Rate (fissions/sec/g)
10-1/2 in. above center	0.4781	1.092×10^6
9 in. above center	0.5846	1.335×10^6
6 in. above center	0.7986	1.823×10^6
3 in. above center	0.9572	2.185×10^6
Center position	1.000	2.283×10^6
3 in. below center	0.9774	2.231×10^6
6 in. below center	0.8172	1.866×10^6
9 in. below center	0.6011	1.372×10^6
10-1/2 in. below center	0.5005	1.143×10^6

Appendix F

COMPARISON OF THE FISSION RATE DISTRIBUTION WITH THE THERMAL FLUX DISTRIBUTION

After the fission rate at various positions along the fuel element was determined (Appendix E), it was necessary to determine the total fission rate in the special assembly. As described in Part II[1] gold foils were exposed on all four sides of the special fuel element and at corresponding positions on the removable center fuel plate. Data was taken at the center position and at points above and below the center position. This data was used to find an average thermal flux all along the element. The results are given in Table F-1.

Table F-1. Average of Thermal Flux Measurements on Center Plate and Four Sides of Special Fuel Element (Data taken from Part II[1])

Position on Element	Average Thermal Flux (neutrons/cm^2/sec)
Center position	1.719×10^6
3 in. above center	1.627×10^6
3 in. below center	1.626×10^6
6 in. above center	1.364×10^6
6 in. below center	1.375×10^6
9 in. above center	1.013×10^6
9 in. below center	1.016×10^6
10-1/2 in. above center	8.09×10^5
10-1/2 in. below center	8.42×10^5
12 in. above center	1.051×10^6
12 in. below center	1.057×10^6

The average thermal flux values were plotted as shown in Fig. 5. Integrating numerically under this curve, it was found that the average thermal flux for the entire element was 1.3265×10^6.

On the center plate of the special element gold foils were exposed at the same positions the U-Al discs had been exposed. The thermal flux was computed for these positions by use of the gold foil data for comparison with the fission rate (see Table F-2).

The average ratio of the fission rate to the thermal flux along the entire fuel element was found to be 1.381. This ratio, when applied to the average thermal flux for the element, determined the average fissions per second per gram for the element.

Table F-2. Comparison of Fission Rate with Thermal Flux at Various Positions along Center Fuel Plate

Position on Plate	Thermal Flux (neutrons/cm^2/sec)	Fission Rate (fissions/sec/g)	Ratio
Center position	1.669×10^6	2.283×10^6	1.368
3 in. above center	1.618×10^6	2.185×10^6	1.350
3 in. below center	1.627×10^6	2.231×10^6	1.371
6 in. above center	1.295×10^6	1.823×10^6	1.408
6 in. below center	1.348×10^6	1.866×10^6	1.384
9 in. above center	$9.65[illegible] \times 10^5$	1.335×10^6	1.384
9 in. below center	1.001×10^6	1.372×10^6	1.371
10-1/2 in. above center	7.702×10^5	1.092×10^6	1.418
10-1/2 in. below center	8.29×10^5	1.143×10^6	1.378
		Avg.	1.381

Appendix G

CONSTRUCTION AND CALIBRATION OF THERMOCOUPLES

Calibrated thermocouples were used for the measurements of the temperature rise ΔT of the water flowing through the fuel elements. The thermocouples were made with Leeds and Northrup B and S No. 30 iron-constantan wire with glass insulation. In the actual assembly several limiting factors existed, among which the following seemed the most important:

(1) The points of measurement were under 15 ft of water.

(2) The points of measurement were in a field of high flux.

(3) A high-temperature gradient existed close to the point of measurement.

(4) Introduction of small amounts of certain materials close to the fuel plates would affect the reactor operation.

These limiting features were kept in mind when the thermocouples were assembled as shown in Fig. G-1. Each thermocouple was made by pulling 30 ft of iron-constantan wire through 23 ft of 1/4-in. OD gum rubber tubing. A 5-in. length of stainless steel tubing

UNCLASSIFIED
DWG 19177

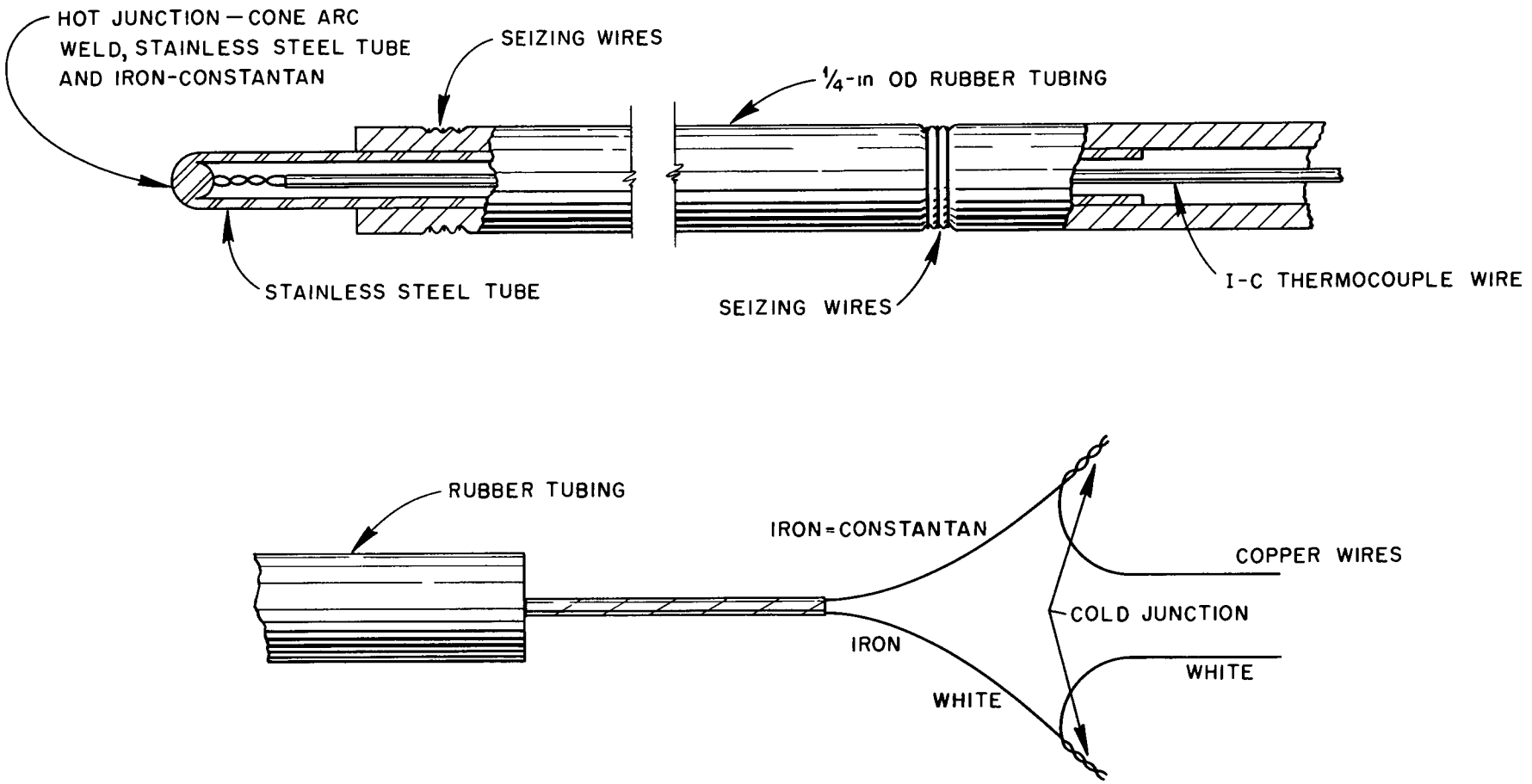

Fig G-1 Thermocouple Construction

(100-mil OD and 10-mil wall) was slipped over the ends of each pair of thermocouple wires which had been cleaned and twisted in the conventional manner. The wires were then cone-arc welded in a bead with the end of the stainless steel tubing to make the hot junction.

The hot junction was checked with an ice cube to make certain that the point of maximum response was at the tip of the stainless steel tubing. After this test the rubber tubing was slipped over the stainless steel tubing and secured with seizing wire in two places, leaving about 1/2 in. stainless steel tubing exposed.

The cold junction (Fig. G-1) was made by soldering the other end of the thermocouple wire to No. 30 gage copper wire and coating the junction and several inches of each wire with red glyptol.

Each thermocouple was checked for several features before further assembly. Leak testing was performed under water by applying 10 psig to the open end of the rubber tubing. Following this, both the hot and cold junctions were immersed in an ice bath to check for a zero reading on a sensitive galvanometer.

After these tests each couple was assembled in some particular adapter. In all, five types of adapters held the thermocouples at

points where measurements were desired. The important adapters were the ones for the special element. In Fig. G-2 one of the hot-junction couples in the top adapter assembly for the special element is shown in its final position. The rubber-covered stainless steel tubing was forced through the small opening in the aluminum cap, giving a watertight seal. The stainless steel tubing was shaped slightly to position the couple in the fluid stream, and the rigid tubing was anchored in two places so the thermocouple would not move during the test.

Four thermocouples, three of which were connected in a thermopile arrangement, were equally spaced around the cone-shaped reducer in the aluminum adapter. The two gaskets and the lucite adapter shown in Fig. G-1 were used to mount the metal adapter to the special fuel element without any metal to metal contact in order to keep heat conduction losses to a minimum. When mounted in the top of the special element the adapter assembly was airtight for pressures of 10 psig.

The adapter used for the bottom of the special element is shown in Fig. G-3. Basically this adapter was simply a modified version of the standard base plug for a regular BSR fuel assembly.

UNCLASSIFIED
DWG 19178

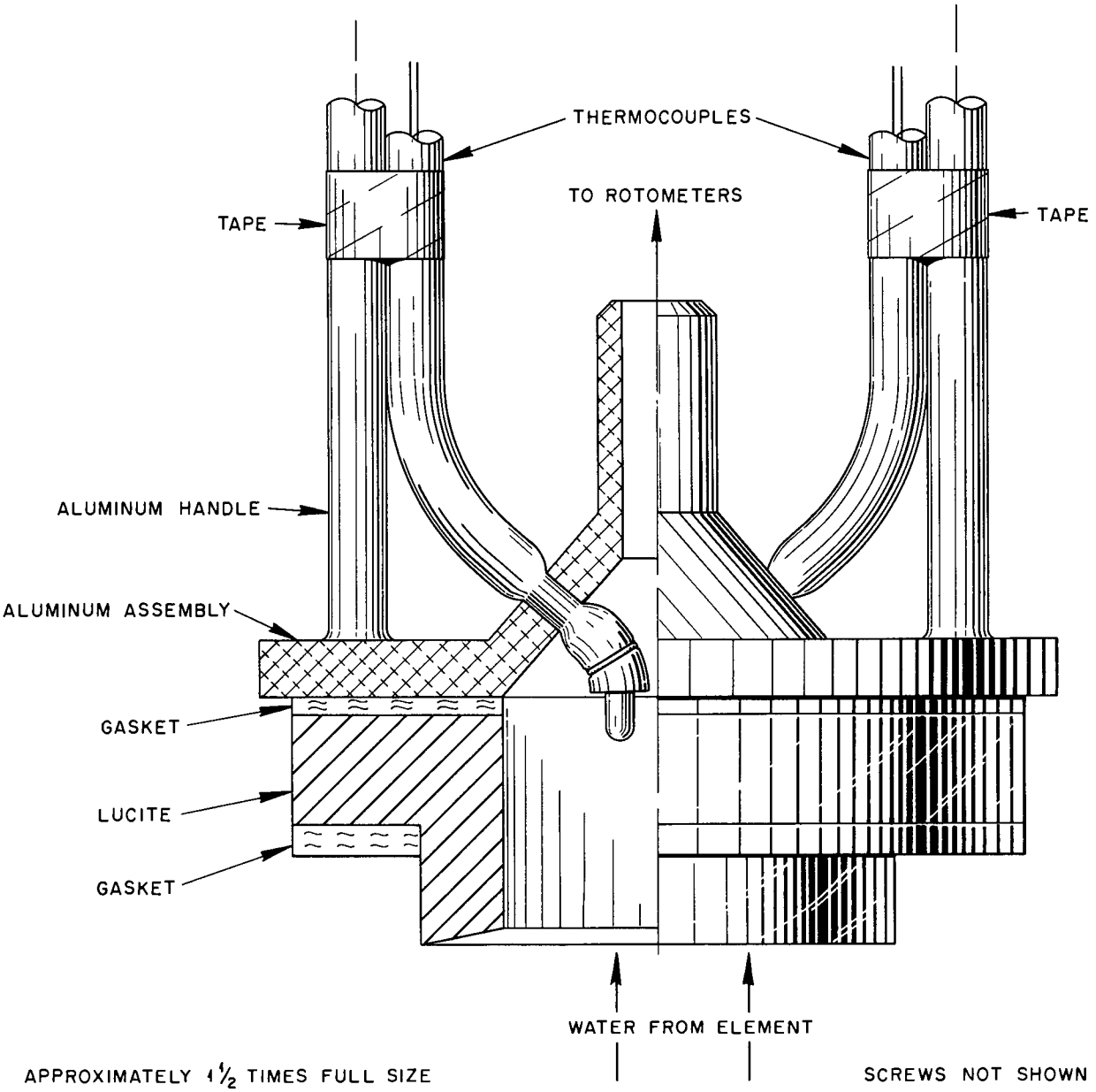

Fig G-2 Thermocouple Adapter Assembly for Top of Special Element

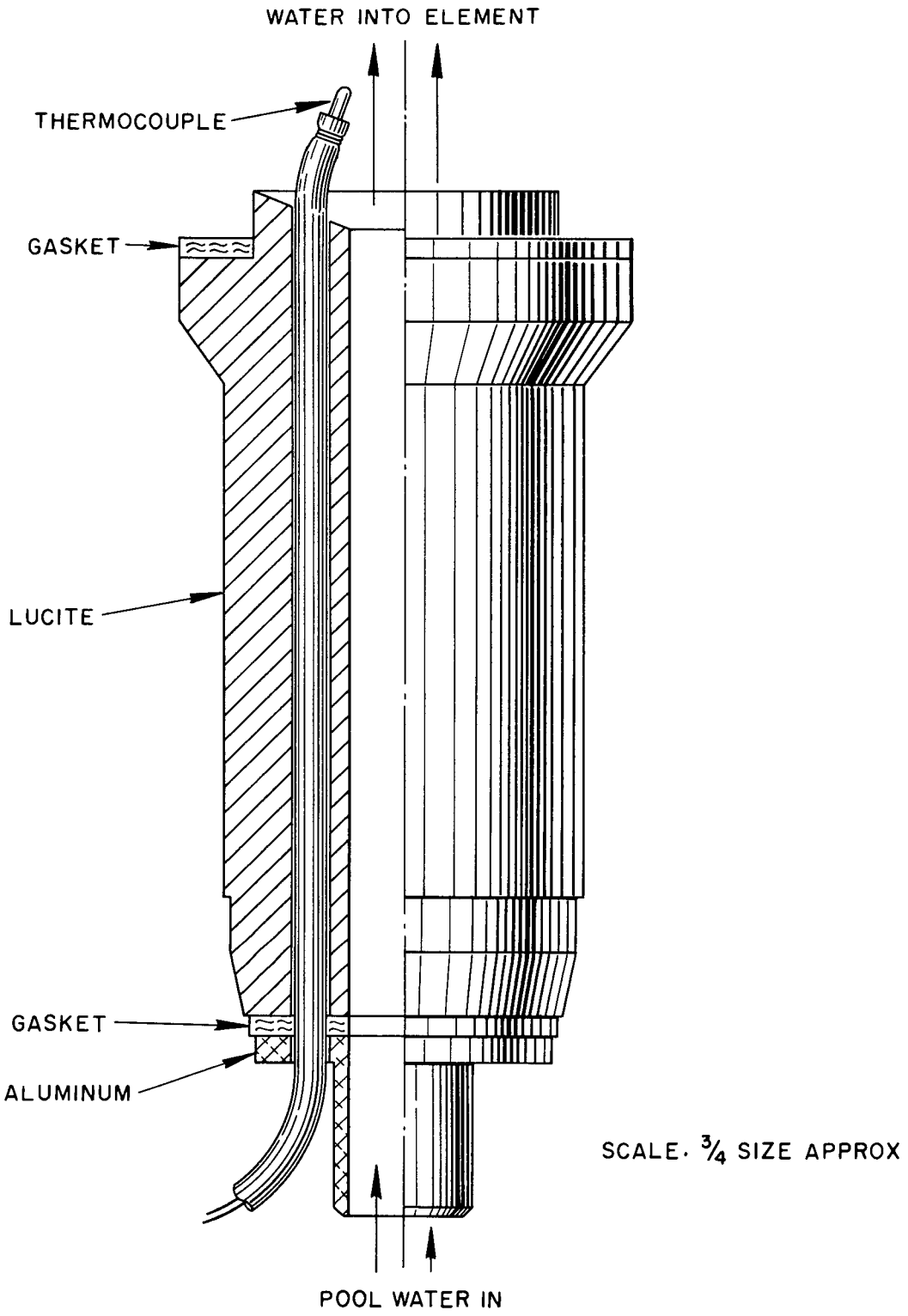

Fig G-3. Thermocouple Adapter for Bottom of Special Element.

Four features differentiate it from the standard base plug: (1) The material used was lucite instead of aluminum, again for the purpose of minimizing heat conduction; (2) the plug was removable and when assembled as shown made the fuel element completely airtight; (3) uniformly spaced holes were drilled through the length of the plug to hold the four thermocouple leads; (4) a special adapter at the bottom end of the base plug sealed the opening around the thermocouple wires and provided a method of attaching a tube to pump the water through the element at a constant rate as desired.

Adapters for the regular elements were basically the same as the metal assembly shown for the top of the special element. These metal assemblies each contained only two thermocouples, and, complete with gaskets, were held in place on the regular fuel assemblies by hooks which clamped to the lifting rod. No lucite adapters were used in these assemblies.

Other types of adapters held thermocouples in position over open fuel elements and beneath the reactor, but their construction is of no consequence to the experiment.

As noted before, the initial check point for the calibration of the thermocouples was to see if each thermocouple zeroed against its cold junction in the ice bath. Any thermocouple that gave an error of 0.0052 mv (0.1°C) was not acceptable. Since the pool temperature was constant, a second calibration point was obtained by comparing the readings of all the couples at a point 10 ft below the surface. Any couple that gave a reading that differed from the average reading of the couples by as much as 0.005 mv was not acceptable.

To further test the thermocouples, a dummy element (Fig. G-4) was constructed to simulate operating conditions, exclusive of the high neutron flux. This element was used both to give constant temperatures for calibration and to provide an endurance test for the thermocouples on the special element. The operating conditions were simulated by connecting the thermocouple adapters to the dummy element complete with water flow tube and thermocouples. Water flow through the element was maintained at a constant rate and the water was heated by means of a calrod heater.

For the calibrations the thermocouple arrangement was such

UNCLASSIFIED
DWG 19180

APPROX ¼ SIZE

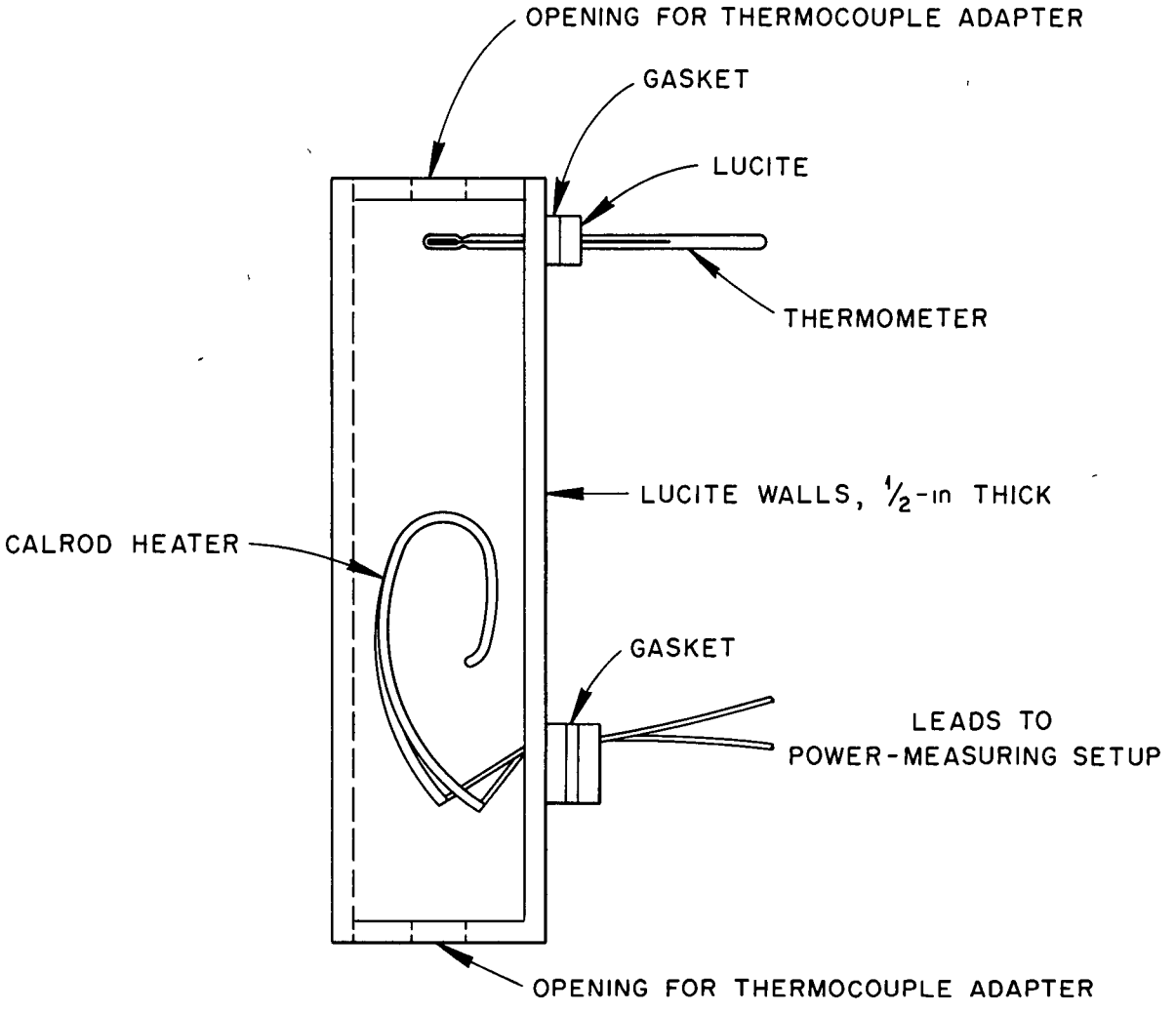

NOTE DURING RUNS, DUMMY COVERED WITH 4 in COTTON

Fig G-4 Dummy Element Without Insulation or Thermocouple Adapters

that each couple could be read versus its cold junction in the ice bath or versus another thermocouple to give a differential reading.

In the endurance test eight thermocouples were connected in a thermopile arrangement to give four times the temperature difference across the dummy element. The water flow was maintained at 1500 cc/min for a period of a month. During this time power was supplied to the element about 1/4 of the time and a Brown recorder was used to note any large temperature changes. Actual readings were taken with a type K potentiometer and a sensitive galvanometer. Under these conditions the initial thermopile millivolt readings were 0.0000 mv for a zero power input and 1.1645 mv for a 600-watt input; after one month the millivolt readings were 0.0020 for zero power input and 1.1682 for a 600-watt input.

Appendix H

INSTALLATION AND CALIBRATION OF ROTOMETERS

The equipment used to ensure constant water flow through the fuel elements is sketched in Fig. H-1. Water was drawn from the pool into the bottom of the fuel element, out through a tube connected to the top of the element, up through a rotometer, and then to an aspirator.

Before the five rotometers were calibrated they were mounted on a rack and placed in the same positions in which they would be used when finally connected to the special fuel element and the four surrounding elements, respectively. In each case, a chamber was attached to the water line to trap all air bubbles before they reached the rotometer. As can be seen in Fig. H-1, valve 2 was used to control the amount of water flow from the fuel element. After each reading valve 1 was opened and the air chamber was purged of the trapped air without changing the total flow from the fuel element. Valve 1 was then closed and the rotometer again carried all the water flow. In this manner constant flow was maintained without fluctuations caused by air bubbles.

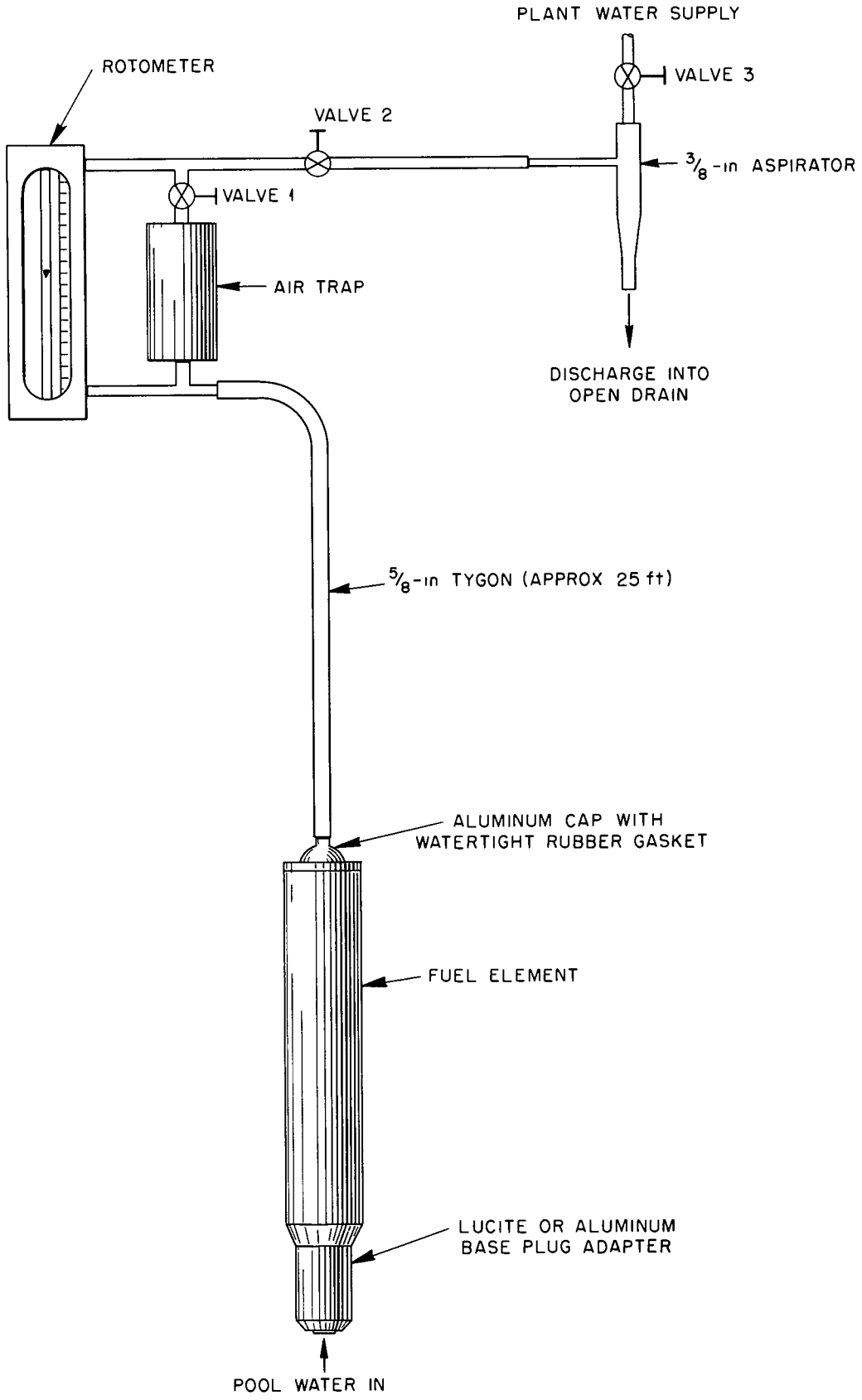

Fig H-1 Apparatus for Maintaining Constant Water Flow Through Fuel Element

With the above arrangement water from a constant head was allowed to pass through each rotometer for various settings on the scale and the time required to fill a calibrated 20,000-ml container was noted. The flow rates obtained are tabulated in Table H-1.

Table H-1. Rotometer Calibrations

Nominal Flow (cc/min)	Flow Rate Through Rotometer (cc/min)				
	At Position 37	At Position 27	At Position 36	At Position 47	At Position 38
500	503	505	507	504	
750	742	746	744	750	733
1000	1002	999	999	1005	1007
1250	1252	1254	1266	1264	1264
1500	1500	1517	1547	1513	1529
1750	1735	1768	1807	1754	1799

Appendix J

INSTALLATION OF THERMOCOUPLES AND WATER TUBES

After the thermocouples were calibrated (see Appendix G) the adapters with the necessary gaskets were assembled on the fuel elements. Since the elements which were to surround the special element were hot (highly radioactive), it was necessary to equip them with adapters under water with special tools. The special element, of course, was cold for this assembly. (An exploded view of the special element is shown in Fig. 2 of the text.) After the adapters were installed, each element was suspended in the pool and air pressure was applied to the water flow connection leading to the top of the element. Enough pressure was applied to force the water out and to check the element for leaks. Each element was tested in this manner before assembly in the reactor.

As noted in the text, water pump grease was used to eliminate water flow between the special element and the adjacent elements. Since the special element was the only cold element to be used in the final loading, the reactor was unloaded and the pool was drained for its location in the reactor grid. Grease was carefully applied to the surface of the special element after which cold fuel elements

were temporarily placed around it to insure that all spaces between the elements were filled. The cold elements then were removed and the pool water was raised to a level which was safe but low enough for the careful installation of the hot elements adjacent to the special element. The pool was then filled, the reactor loading was completed, and the thermocouple leads and water flow lines were connected for operation. (The water flow system is described in Appendix H.)

A simplified layout of the thermopile leads to the special element is shown in Fig. J-1. In this setup the millivolt reading was proportional to three times the temperature rise across the element. Provisions were also made so that each of the six couples in the thermopile could be read separately by means of switches in the copper lines leading from the ice baths. In a similar manner any couple in the top of the element could be read against any couple in the bottom, giving the temperature rise through the element as seen by one pair of thermocouples. In the other elements the differential readings were taken by reading each couple versus one in the bottom of the special element. Differential readings taken with couples in the base of the special element versus couples in the water under the reactor gave no

UNCLASSIFIED
DWG 19181

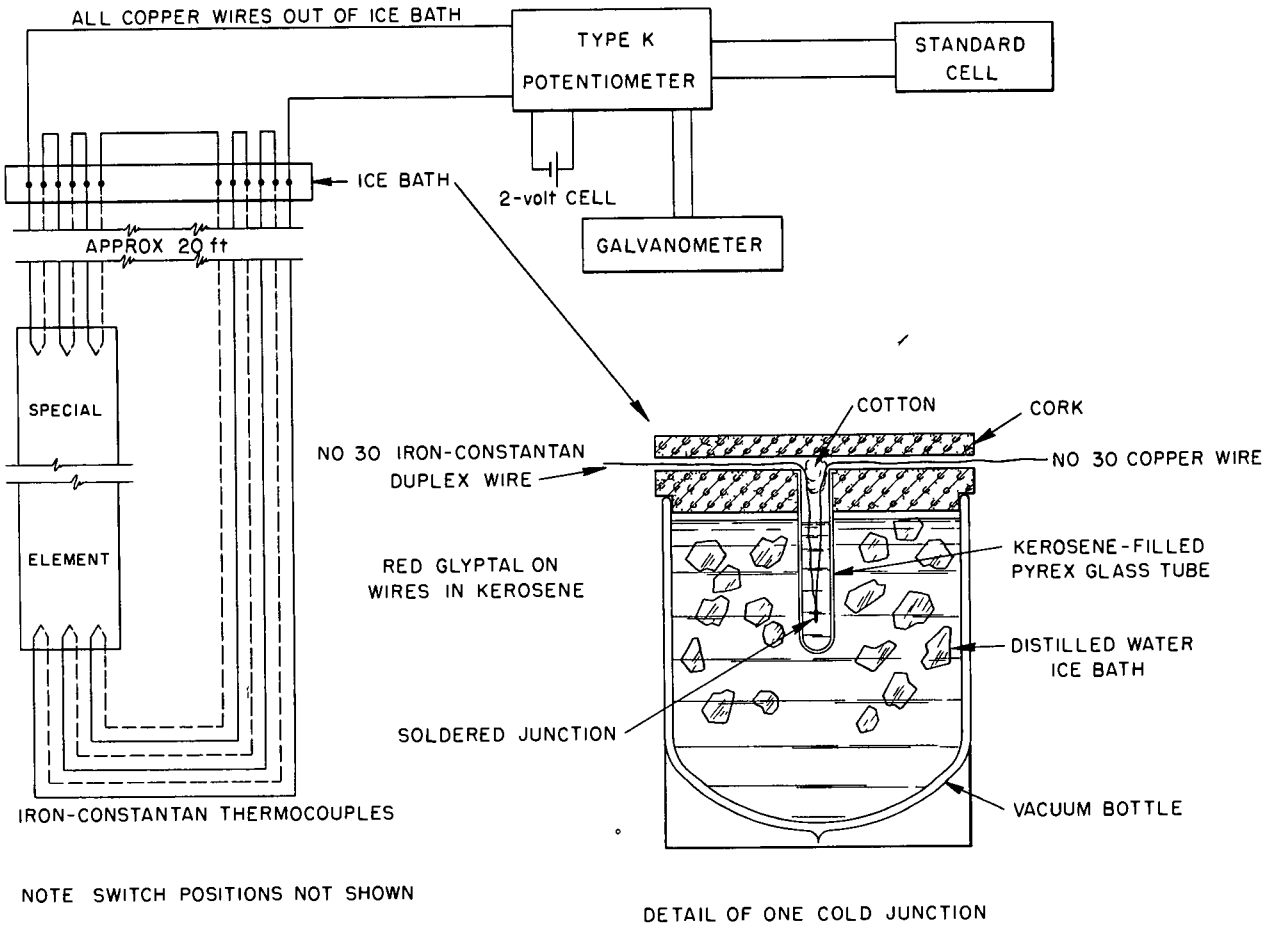

Fig J-1 Thermopile Arrangement in Special Element

temperature difference for the power levels over which the experiment was conducted.

Each day before reactor start-up, all the couples were checked to see if they read the same temperature.

Appendix K

DATA FOR THE DETERMINATION OF THE POWER IN THE SPECIAL ELEMENT

Before the power in the special element could be determined it was necessary to measure the difference between inlet and outlet temperatures of water forced through the special element at a given rate. The water flow through the four surrounding elements (positions 27, 36, 38, and 47 in Fig. 1 of the text) was regulated so that the temperature rise through these elements was very nearly the same as the temperature rise through the special element. (See Appendixes G, H, and J for descriptions of the installation of water tubes and thermocouples in the fuel elements.) This minimized any heat transfer from the special element to the surrounding elements. To further minimize any heat transfer, water pump grease was packed on all four sides of the special fuel element.

Runs were made with water flows through the special element approximating 1000,1500, and 1750 cc/min. During each run the reactor power was varied over a considerable range, and at each new power setting it was allowed to operate for at least 1/2 hr.

Longer operating periods did not give further variations in temperature.

The data on the special element (position 37) are given in Table K-1 and the data on the four surrounding elements are given in Tables K-2 and K-3. The temperature rise in the special element was read from the difference in EMF between a thermocouple in the bottom of the element and another in the top. In addition, three such pairs were connected in series to form a thermopile as described in Appendix J. It was found that readings on this thermopile could be repeated to within 0.2°C, which was the limiting sensitivity of the potentiometer. All calculations were based on the temperature difference measured with the thermopile. The other pair of thermocouples was used only as a monitor.

The product of the water flow W times the temperature rise ΔT divided by the reactor power P should be constant. Inspection of Table K-1 shows that within reasonable error $W\Delta T/P$ is constant. During the three runs reported the operation of the reactor and its controls and the performance of the water-flow and temperature-measuring equipment was such as to give complete confidence in the data. No other uncertainty could compare with the uncertainty of

the 0.2°C in the temperature difference readings. Accordingly a percent error for each reading equal to 0.2/ΔT was calculated, and using this percent error the absolute error in WΔT/P was computed. A plot of WΔT/P versus reactor power for the three runs is shown in Fig. 6 of the text. By properly weighting the points according to the individual errors, the best value of WΔT/P was found to be 1089 ± 10 cal/g-kw.

At the conclusion of run 69, where the reactor power was 27.38 kw and the water flow through the special element was approximately 1750 cc/min, the water flow through the element in position 38 was raised from 1000 to 1800 cc/min and the temperature rise in the special element was observed. The ΔT changed from 16.83 to 16.80°C, a difference barely noticeable. Similarly, when the water flow through the element in position 38 was decreased to 525 cc/min the ΔT in the special element was 16.88°C. This data gave convincing evidence that the net heat loss or gain from the special fuel element to its surroundings was negligible. Although the water flow in the four surrounding elements had been closely regulated throughout the experiment so as to give the same temperature rise as through the

special element, such precautions really had not been necessary.

One further reading of run 69 (Tables K-2 and K-3) was taken with a water flow through the special element of 1240 cc/min, the water flow through the surrounding elements again being regulated so that the temperature rise across them was approximately the same as across the special element. Since the value of $W\Delta T/P$ agreed with that obtained from the three preceding runs, no further readings at this water flow were taken and the experiment was concluded.

One fuel element (position 25) had been equipped with thermocouples but the water was allowed to flow through it by natural convection during the experiment. Data on the temperature rise through that element is included in Table K-3. Because of the uneven flow of water with natural convection, the temperature readings oscillated badly and are therefore only approximate.

Table K-1. Temperature Rise and Water Flow Through Special Fuel Element, Position 37

Nominal Reactor Power, P (kw)	Actual Water Flow, W (cc/min)	Temperature Rise, ΔT(°C)		$W\Delta T/P$		
		Thermocouple Reading	Thermopile Reading	(cal/g-kw)	Percent Error	Absolute Error (±)
Run 64, Water Flow Approximately 1000 cc/min						
2.190	1000	2.3	2.387	1090	8.379	91
3.833	1005	4.1	4.213	1105	4.747	52
5.475	1000	5.9	6.046	1104	3.308	37
7.665	1005	8.1	8.177	1072	2.446	26
10.95	1017.5	11.9	11.95	1104	1.674	18
15.33	1015	16.6	16.66	1103	1.200	13
Run 68, Water Flow Approximately 1500 cc/min						
3.833	1500	2.8	2.846	1114	7.03	78
5.475	1500	3.9	4.013	1099	4.98	55
7.665	1502.5	5.6	5.623	1102	3.56	39
10.95	1500	8.0	8.003	1096	2.50	27
15.33	1500	11.1	11.15	1091	1.79	20
21.90	1487.5	13.8 should be 15.8 ccw	15.88	1079	1.26	14
Run 69, Water Flow Approximately 1750 cc/min						
3.833	1735	2.5	2.469	1118	8.10	91
5.475	1732.5	3.5	3.489	1104	5.73	63
7.665	1735	4.9	4.889	1107	4.09	45
10.95	1750	6.8	6.879	1099	2.91	32
15.33	1745	9.5	9.5	1082	2.10	23
21.90	1750	13.7	13.52	1080	1.48	16
27.38	1750	16.8	16.83	1076	1.19	13
Run 69, Water Flow 1240 cc/min						
13.69	1240	12.0	12.1	1092	1.66	18

Table K-2. Temperature Rise and Water Flow Through Elements in Positions 36 and 38 Adjacent to Special Element

Nominal Reactor Power, P (kw)	Position 36		Position 38	
	Actual Water Flow, W (cc/min)	Temperature Rise,[a] ΔT (°C)	Actual Water Flow, W (cc/min)	Temperature Rise,[a] ΔT (°C)
Run 64, Water Flow Through Special Element (Position 37) Approximately 1000 cc/min				
2.190	1225	2.1, 2.1	925	2.2, 2.1
3.833	1010	4.0, 4.1	725	4.4, 3.8
5.475	945	5.8, 5.9	525	6.6, 6.2
7.665	900	8.2, 7.9	500	8.6, 8.2
10.95	775	11.8, 11.9	420	12.5, 11.8
15.33	735	16.8, 17.1	415	17.1, 15.9
Run 68, Water Flow Through Special Element (Position 37) Approximately 1500 cc/min				
3.833	1660	2.8, 2.9	1050	3.5, 2.9
5.475	1605	3.8, 3.9	1000	4.9, 3.9
7.665	1550	5.4, 6.8	980	6.8, 5.6
10.95	1460	7.7, 7.8	910	9.5, 8.1
15.33	1380	10.8, 11.0	815	12.56, 11.1
21.90	1260	15.7, 15.9	780	17.1 15.8
Run 69, Water Flow Through Special Element (Position 37) Approximately 1750 cc/min				
3.833	2000	2.4, 2.5	1330	3.0, 2.4
5.475	1900	3.5, 3.5	1240	4.3, 3.5
7.665	1790	4.9, 5.0	1200	5.9, 4.9
10.95	1775	6.6, 6.7	1200	7.9, 6.9
15.33	1675	9.5, 9.6	1150	11.0, 9.5
21.90	1650	13.1, 13.3	1010	15.2, 13.6
27.38	1550	16.4, 16.7	1000	18.3, 16.6
Run 69, Water Flow Through Special Element (Position 37) 1240 cc/min				
13.69	1050	- 12.0	625	- 11.7

(a) Dual readings reported as given by two thermocouples in top of each element.

Table K-3. Temperature Rise and Water Flow Through Elements in Positions 25, 27, and 47 Adjacent to Special Element

Nominal Reactor Power, P (kw)	Position 25	Position 27		Position 47	
	Temperature Rise,[a] ΔT(°C)	Actual Water Flow, W (cc/min)	Temperature Rise,[a] ΔT (°C)	Actual Water Flow, W (cc/min)	Temperature Rise,[a] ΔT(°C)
Run 64, Water Flow Through Special Element (Position 37) Approximately 1000 cc/min					
2.190	1.6, 2.5	1145	2.1, 2.1	1000	2.1, 2.1
3.833	4.0, 3.5	990	4.0, 4.0	850	4.1, 3.9
5.475	4.5, 4.5	915	5.8, 5.8	750	5.9, 5.5
7.665	5.4, 5.7	810	8.6, 8.3	750	8.1, 7.9
10.95	6.9, 6.7	715	12.0, 12.1	610	12.0, 11.7
15.33	8.2, 7.9	650	17.0, 17.0	540	16.4, 16.7
Run 68, Water Flow Through Special Element (Position 37) Approximately 1500 cc/min					
3.833	4.1, 3.9	1670	2.7, 2.8	1400	2.8, 2.7
5.475	4.9, 4.8	1540	3.8, 3.9	1320	3.9, 3.8
7.665	5.4, 5.3	1525	5.3, 5.3	1280	6.8, 5.4
10.95	7.0, 6.6	1400	7.9, 7.9	1180	8.1, 7.8
15.33	8.0, 7.7	1320	11.1, 11.0	1060	11.4, 11.1
21.90	9.6, 9.4	1255	16.0, 14.9	1010	16.1, 16.0
Run 69, Water Flow Through Special Element (Position 37) Approximately 1750 cc/min					
3.833	4.0, 4.0	1900	2.4, 2.4	1830	2.4, 2.3
5.475	5.0, 1.9	1825	3.5, 3.5	1550	3.5, 3.4
7.665	5.8, 5.3	1800	4.8, 4.8	1465	5.0, 4.9
10.95	6.9, 6.7	1730	6.6, 6.7	1440	6.9, 6.7
15.33	8.1, 8.0	1610	9.5, 9.5	1450	9.4, 9.2
21.90	9.6, 9.2	1670	13.0, 12.8	1310	13.3, 13.1
27.38	10.3, 10.3	1475	17.0, 16.0	1260	16.4, 16.8
Run 69, Water Flow Through Special Element (Position 37) 1240 cc/min					
13.69	- 7.5	1015	12.2 -	850	- 11.7

(a) Dual readings as given by two thermocouples in top of each element.

Appendix L

NET LEAKAGE OF RADIATION INTO SPECIAL FUEL ELEMENT

Referring to Hanna's paper,[2] it is possible to estimate the fraction of the total energy per fission which was given off in the form of neutrons and gamma rays. The neutrinos completely escaped detection, and it was assumed that none of the fission fragments and beta particles leaked out of the special element. It was possible for some neutrons and gamma rays to leak out, but the reactor was so loaded that a nearly compensating number of these particles should leak into the special element from the surrounding elements.

The net leakage out of the special element in position 37 was four times the leakage out of one side plus twice the leakage out of one end minus the leakage in through the side from each of the four surrounding elements, or:

$$L = 4L^{37}_{sides} + 2L^{37}_{ends} - (L^{36}_{side} + L^{38}_{side} + L^{27}_{side} + L^{47}_{side})$$

The gamma leakage out one side of the special element is:

$$L^{37}_{side} = \frac{1}{6}\int_{o}^{Z_1} \frac{E_{tot}}{V} A \frac{E_\gamma}{E_F} e^{-Z/\lambda_\gamma} dZ$$

where

E_{tot} = total energy generated in the special element,

V = volume of special element,

A = area of one side,

$\frac{E_\gamma}{E_F}$ = fraction of fission energy in the form of gammas,

λ_γ = gamma relaxation length,

Z_1 = width of fuel element,

$\frac{1}{6}$ = fraction of radiation traveling in the Z direction.

Numerically,

$V = 3540\ cm^3$,

$A = 465\ cm^2$,

$\frac{E_\gamma}{E_F} = 0.063$ (see Ref. 2),

$\lambda = 11.5$ cm,

$Z_1 = 7.62$ cm.

Thus

$$L^{37}_{side} = 7.68 \times 10^{-3}\ E_{tot}$$

This simply means that of the total energy generated in the special element 0.768% leaked out through one side in the form of gamma rays.

The leakages into the special element from positions 38 and 47 were calculated indentically except for the correction in total energy generated in those elements (see Table B-9 in Part II). In calculating the leakage across the interface from element 36 into element 37 and also from element 27 into element 37, allowance was made for radiation originating in fuel elements further away in the reactor (see Fig. 1). The same general method was used to calculate the leakage out of the top and bottom of the special element. In this case the energy density, $\frac{E_{tot}}{V}$, could no longer be assumed constant in the integration but was considered to vary directly as the thermal neutron flux (see Fig. 5). The net gamma leakage was found to be:

$$L_\gamma = -0.14\%$$

where the minus sign denotes that the net leakage was into the special element.

The fraction of the fission energy appearing in the form of neutrons, $\frac{E_n}{E_F}$, is 0.025 and a neutron relaxation length, λ_n, of 4.5 cm was used. The net neutron leakage was much smaller than the gamma leakage

$$L_n = -0.03\%$$

As a result, the net radiation leakage into the special element was 0.17%, an almost negligible quantity.

REFERENCES

1. J. L. Meem and E. B. Johnson, Determination of the Power of the Shield Testing Reactor, Part I, ORNL-1027 (Aug. 13, 1951); E. B. Johnson and J. L. Meem, Determination of the Power of the Bulk Shielding Reactor, Part II, ORNL-1438 (April 21, 1953).
2. G. C. Hanna, CRR-489 (May 18, 1951).
3. R. B. Leachman, "Velocities of Fragments from Fission of U^{233}, U^{235}, and Pu^{239}," Phys. Rev. 87, 444 (1952).
4. E. D. Klema, R. H. Ritchie, and G. McCammon, ORNL-1398 (Oct. 17, 1952).
5. C. D. Smith, F. W. Drosten, and F. Kerze, Jr., ORNL-951 (April 9, 1951).
6. J. E. Cunningham, CF-52-6-54 (June 10, 1952).
7. T. H. R. Skyrme, MS-91 (1947).